Hydrogen Effects on the Point Defect Spectrum in Fe-C Alloys

By

Paul Rene Monasterio Velásquez

Submitted to the Department of Nuclear Science and Engineering in Partial Fulfillment of the Requirements for the Degree of

Master of Science in Nuclear Science and Engineering

At the

Massachusetts Institute of Technology

[June 2008]

May 2008

Author_____

Department of Nuclear Science and Engineering
May 9, 2008

Certified by_____

Sidney Yip
Thesis Supervisor
Professor of Nuclear Science and Engineering and Materials Science

Certified by_____

Krystyn Van Vliet
Thesis Reader
Professor of Materials Science and Engineering

Accepted by_____

Jacquelyn Yanch
Chair, Department Committee on Graduate Students

Hydrogen Effects on the Point Defect Spectrum in Fe-C Alloys

By

Paul Rene Monasterio Velásquez

Submitted to the Department of Nuclear Science and Engineering on May 9, 2008 in partial fulfillment of the requirements for the Degree of Master of Science in Nuclear Science and Engineering

Abstract

As part of a multi-scale approach for modeling hydrogen embrittlement in hardened steels we have investigated, employing density functional theory methods, the stability and concentrations of the point defect clusters present in metastable Fe-C-H alloys with vacancies. The defect spectrum is found to be strongly dependent on the local vacancy concentration, and for low hydrogen levels sharp highly non-linear changes in the defect cluster population are observed at critical vacancy concentrations. This critical-like behavior suggests an energy activation mechanism which can be characterized by an effective defect-cluster formation energy barrier. By analogy with similar activated processes such as the liquid-to-glass transition in super-cooled liquids, we postulate that this criticality is associated with the presence of deep wells in the energy landscape where chemical composition plays the role of generalized coordinate.

Increases in the hydrogen content have the qualitative effect of reducing the slopes in the defect concentrations. The drastic sensitivity of the defect cluster spectrum to local changes in vacancy and impurity concentrations implies that in proximity of surfaces and extended defects multiple defect clusters become statistically significant and migration dependent phenomena, such as creep—relevant to hydrogen embrittlement—and super-diffusion, should be controlled by multiple activation barriers.

Thesis Supervisor: Prof. Sidney Yip

Contents

Abstract **3**

Contents **4**

Acknowledgments **5**

List of Figures **6**

List of Tables **7**

1. Introduction **8**

2. Hydrogen Damage in Metals **12**

2.1. Hydrogen Sources 13

2.2. Thermodynamics of Hydrogen-Metal Systems 14

2.3. Hydrogen Embrittlement in Steels 19

2.4. Hydrogen Trapping and Blistering 22

2.5. Decarburization and Methane Formation in Steels 24

2.6. Summary 24

3. Point Defect Spectrum in Fe-C-H Alloys **26**

3.1. Point Defects-Hydrogen Interactions in Metals 27

3.2. DFT Calculations of Defect Binding and Stability 32

3.3. Point-Defect Clusters in Fe-C Alloys 38

3.4. Critical Behavior and Activated Processes 41

3.5. Effects of Hydrogen in the Fe-C Spectrum 43

3.6. Bulk vs. Local Effects 53

4. Multi-scale Approach to Embrittlement and Future Work **55**

4.1. Hydrogen Empirical Potentials 55

4.2. Cluster Diffusion and KMC Modeling of Dislocation Climb 56

5. Conclusions **58**

References **60**

Acknowledgments

Throughout my life I have been blessed to have the support of a multitude of people who have contributed in a variety of ways to my development both as a scientist and as a person. Any of my accomplishments would have been impossible without the support provided by the shoulders of the giants of my life.

Thanks go first and foremost to my research advisor, Prof. Sidney Yip, for his support and mentoring during the past two years. Through my conversations and interactions with Prof. Yip not only have I enriched my knowledge about materials physics, but I have also learned a great deal about many of the additional aspects of a scientific and academic career. I believe that that knowledge has greatly contributed towards my development as a scientist.

In addition I would also like to thank another great mentor and friend, Prof. Brian Wirth from my alma mater UC Berkeley. Brian has provided me with his full support and trust since I first met him over four years ago and even now continues to be my one of my main sources of advice and support when confusion and indecision make things difficult. Thanks for all your help Brian.

I would also like to acknowledge the other mentors who have played a vital role in my scientific formation throughout the years and who have been key in shaping the pathway I have taken. My deepest thanks go to Prof. Krystyn Van Vliet and Prof. Nicola Marzari at MIT, Dr. Jaime Marian and Dr. Malvin Kalos at the Lawrence Livermore National Laboratory, and Prof. Rafael Sanchez Lamoneda at the Universidad Central de Venezuela.

Also, I want to thank the many friends and colleagues who have always been there to give a hand when I have needed support. To the members of the Yip group: Tim, Xiao, Mukul, and Akihiro, thanks a lot for all your help! I also thank my great friends Kevin, Prateek, Christina, Emilie, and Steve for always being there for me; and finally a huge hug and an immense thank-you to the TBP gang: James, Angela, Pokai, and Diana, you guys rock!

Last, but definitely not least, I would like to thank the most important people in my life and the reason for all of my efforts: my family. I cannot write enough words to thank my mother, sister, and grandmother for their love, unconditional support throughout the years, and for making me the person I am today. To them I dedicate this thesis and all of my work.

List of Figures

Figure 2.1. Variation of the relative partial enthalpy of solution at infinite solute dilution with the group number of solvent metal.

Figure 3.1. Schematic of the approximate locations of the atoms in the configurations corresponding to key defect complexes.

Figure 3.2. Partial point-defect cluster spectrum in Fe-C alloys as a function of total vacancy concentration for $[C_{tot}]=0.01$.

Figure 3.3. Effective activation barriers for key point-defect clusters in Fe-C as a function of total vacancy concentration for $[C_{tot}]=0.01$.

Figure 3.4. Partial point-defect cluster spectrum in Fe-H alloys as a function of total vacancy concentration for $[H_{tot}]=0.01$.

Figure 3.5a,b. Partial point-defect cluster spectrum in Fe-C-H alloys as a function of total vacancy concentration for $[C_{tot}]=0.01$ and $[H_{tot}]=0.001$.

Figure 3.6a,b. Partial point-defect cluster spectrum in Fe-C-H alloys as a function of total vacancy concentration for $[C_{tot}]=0.01$ and $[H_{tot}]=0.01$.

Figure 3.7. Partial point-defect cluster spectrum in Fe-C-H alloys as a function of total hydrogen concentration for $[C_{tot}]=0.01$ and $[V_{tot}]=0.01$.

Figure 3.8. Effective activation barriers for key point-defect clusters in Fe-C-H as a function of total hydrogen concentration for $[C_{tot}]=0.01$ and $[V_{tot}]=0.01$.

List of Tables

Table 2.1. Relative partial enthalpies and entropies for various metallic solvents in dilute solutions.

Table 3.1. Binding energies of H to vacancies relative to H in solution

Table 3.2. Experimental H-solute binding energies in metals relative to H in solution.

Table 3.3. Calculated formation energies for different defect stoichiometries.

Table 3.4. Calculated binding energies for different defect stoichiometries.

Chapter 1

1. Introduction

Hydrogen is ubiquitous in nature. Its presence in almost all environments, ranging from the oceans and atmosphere to modern plasmas, has made it one of the most studied elements in the history of science. Furthermore, its universality combined with high mobility and strong chemical activity makes it one of the most reactive elements in nature and consequently a very powerful agent in modifying the properties of a variety of materials.

For several decades the effects of hydrogen on the properties of materials have attracted attention from a variety of fields. For example, in electronic materials hydrogen is known to play both beneficial and detrimental roles to the properties. It has been used for implantation in amorphous Si to passivate bonds and limit unwanted reactivity [1], and also to mediate the radiation sensitivity in Si and SiO_2 detectors [2]. Furthermore H-containing molecular species are used for layer growth in semiconductors [3] and for stabilizing species in the growth of diamond films [4, 5]. In addition, a variety of fundamentally new phenomena have been observed under hydrogen-rich conditions in metals and their alloys including large volume contractions under high H pressures in some metals including α-Fe [6, 7], enhancement of diffusion at metal-metal junctions [8], and super-lattices of hydrogen-vacancy complexes [9].

Additionally, the problem of hydrogen degradation of the mechanical properties of metals has had significant technological and industrial impact for many years due to the severe embrittlement and delayed fracture experienced by Fe-rich materials such as high-strength

hardened steels [10, 11, and references therein]. Substantial experimental work documenting hydrogen embrittlement in steels under tensile stress is available. The literature focused on this topic alone is vast and encompasses large contributions on energy related technology [12], hydrogen in metals [13], and corrosion [14-18] among others. One case of particular industrial importance is the embrittlement of hardened steels (Fe-C alloys) such as those used for bearings, in which sometimes the operating conditions are such that pickup of atomic hydrogen from the environment is unavoidable. At least two potential plasticity mechanisms have been proposed to explain the experimental evidence of embrittlement in those steels: hydrogen enhanced localized plasticity (HELP) [19-21] and stress relaxation induced by hydrogen-enhanced vacancy populations [11, 22-26].

However, despite many decades of study, a fundamental understanding of the underlying mechanisms that is fully consistent with experimental observations and capable of explaining embrittlement and other hydrogen-induced phenomena, has proven elusive. Nonetheless, in the case of hardened steel the deformation response is intrinsically coupled to the lattice defects in the complex metastable microstructure [27, 28]. In addition, hydrogen-induced changes on the crystal defects structure are collectively considered one of the primary causes for the other observed macroscopic effects. For example, the interaction of hydrogen with vacancies has been deemed responsible for the large volume contraction under high hydrogen pressure experienced by some metals [6,7] and the enhancement of diffusion observed in others [8]. Therefore a predictive and robust model of hydrogen embrittlement and other hydrogen phenomena must be based upon an accurate description of the hydrogen-defects interactions as well as the local effects of the lattice imperfections themselves.

Experimental studies of the defect microstructure in the case of hardened steels have provided insight into the local carbon concentrations [29] as well as the binding energy of the carbon-vacancy cluster [30]; however, they are still unable to resolve the detailed defect microstructure which strongly affects the plastic deformation of the steel. In contrast, a multi-scale modeling approach based on an *ab-initio* understanding of the energy landscape of different point defect clusters has proven successful in predicting self-diffusivities relevant to the creep and fatigue lifetime of hardened bearing steels [27,31,32].

Following a similar approach we present a multi-scale framework to study the hydrogen effects on hardened steels based on three major objectives: to understand the features of the point defect spectrum in Fe-C alloys, to develop fundamental understanding of the interaction of hydrogen with those defects, and finally to determine the properties of the new hydrogen-induced defects and their effects on the local microstructure. In this thesis we limit our scope to the first two goals, and describe a multi-scale approach to tackle the last objective and link the results to more complete embrittlement mechanisms.

The remainder of this thesis is divided into three chapters. The first of these gives an overview on the basic phenomenology and understanding of the effects of hydrogen in metals and metallic alloys with a particular focus on Fe-C alloys. The chapter also discusses the phenomenon of hydrogen embrittlement in steels and motivates the need for a fundamental understanding of the hydrogen-induced changes in the defect microstructure as an essential part in the development of a multi-scale framework to model hydrogen-induced degradation.

The third chapter discusses the main features of the point defect cluster spectrum in the Fe-C-H system from a theoretical perspective by combining density functional theory

calculations with statistical mechanical models to obtain information about the local concentrations of the defect clusters and, in turn, on some of the effects of surfaces and extended defects in the point defect cluster microstructure. In addition, the dramatic threshold behavior observed in the concentrations is studied under the framework of activated processes by making an analogy with the problem of viscosity in super-cooled liquids and proposing a correlation between the threshold behavior and the topology of the energy landscape in a grand canonical ensemble. The effects of hydrogen on the point defect spectrum can then, in principle, be understood as constraints in moving along the energy landscape correlated with fundamental physical mechanisms.

In the final chapter a multi-scale methodology based on the observations of the defect structure is proposed. The multi-scale framework couples atomistic understanding of migration barriers and defect physics to kinetic Monte Carlo modeling of diffusion and creep to provide a more complete picture in the problem of embrittlement.

Chapter 2

2. Hydrogen Damage in Metals

Hydrogen, with only a single proton in the nucleus, is so small that it migrates readily through the crystal structure of most metals and their alloys. For example, the activation energy for diffusion of hydrogen in BCC iron has experimentally been found to be 0.0713 eV and as such hydrogen can diffuse quite rapidly even at relatively low temperatures [10]. Furthermore, its broad range of chemical reactivity magnifies its ability to drastically modify the properties of its host material causing, in many cases, severe detrimental effects.

Hydrogen damage includes a number of those phenomena which degrade the mechanical and metallurgical properties of the metal as a result of the dissolution of hydrogen (atomic or molecular) into the crystalline lattice structure [33]. For instance, initial hydrogen entry as a lattice impurity can produce hydrogen embrittlement in the form of hydrogen-induced cracking in hardened iron alloys because of the restricted slip capabilities in the BCC structure which is prevalent in such steels. In reactive metals, such as titanium, niobium, vanadium and zirconium, hydrogen can also form hydride compounds in the lattice with much lower ductility than the host matrix. Finally, excess atomic or molecular hydrogen in the lattice can congregate and form larger defects such as traps and blisters which generate mechanical stresses inside the material degrading its effective mechanical properties.

Hydrogen damage was first observed by Johnson in 1875 [34], who reported that hydrogen in iron and steels causes a reduction in ductility and fracture stress. In addition, it has been shown

that hydrogen can cause the fracture mode to change from ductile trans-granular to trans-granular cleavage or brittle inter-granular failure [35], similar to the effect of halides in stress corrosion cracking (SCC) which is another phenomenon yet to be fully understood. Numerous mechanisms have been proposed to explain the deleterious effect of hydrogen on the mechanical properties of metals but despite many decades of study many questions remain unanswered. The most commonly cited mechanisms include the hydrogen pressure buildup mechanism [36], hydrogen absorption at the crack tip or surface imperfections [37-39], hydrogen reduction of the cohesive strength of the lattice [40-41], hydrogen accumulation at precipitates and second-phase particles [42-44], formation and fracture of a brittle hydride in reactive metals [45], hydrogen-induced reduction in the stacking-fault energy [46,47], and hydrogen enhanced localized plasticity [35, 48-50].

2.1. Hydrogen Sources

Hydrogen can be made available to a metal surface or bulk from a variety of sources. At high enough temperatures atmospheric hydrogen can spontaneously diffuse to metallic surfaces and localized defects such as cracks, thereby dramatically increasing the local hydrogen concentration. In aqueous environments the cathodic reduction of water also represents an important hydrogen source relevant to many industrial processes involving corrosion or cathodic protection. In addition, the use of hydrogen as a chemical fuel [51-54 and references therein] and its isotopes as nuclear fusion fuels in magnetic confinement reactors constitute a growing arena in which large hydrogen sources are made available to metallic interfaces and in which the hydrogen-metal interactions are of growing interest.

Examples of metal interaction with hydrogen-bearing atmospheres can be found in heat treating, welding, and other manufacturing processes such as bearing in hardened steels. Water

vapor and steam may be decomposed to hydrogen at hot surfaces during welding or heat treating, either providing hydrogen for immediate failure during the exposure or conspiring to produce delayed failure in combination with previous hydrogen exposure.

In addition, cathodic reactions involving hydrogen such as:

$$2H^+ + 2e^- \rightarrow H_2 \tag{2.1.1}$$

$$2H_2O + 2e^- \rightarrow H_2 + 2OH^- \tag{2.1.2}$$

may be present during corrosion, cathodic protection, catalysis, and a variety of other industrial processes. Hydrogen enters the lattice as atomic or nascent hydrogen, which is an intermediate in the formation of molecular H_2 on the surface [33]. Dissolved "poisons" such as phosphorous, arsenic, and sulfur, which retard the formation of molecular H_2 and increase the residence time of nascent hydrogen on the surface, enhance hydrogen entry and increase hydrogen damage.

2.2. *Thermodynamics of Hydrogen-Metal Systems*

The solubility of hydrogen in a metal or metallic alloy is an important variable in determining the thermodynamic behavior of the system. However, due to the extreme properties of hydrogen discussed previously H-solubility data with respect to H_2 gas varies widely from system to system. A convenient way to discuss the variation in H-solubility is to consider the solubility at infinite dilution. In this case, and assuming quasi-regular solutions, it is possible to write [55]:

$$ln\theta = -\frac{\Delta\bar{H}_H^{\infty}}{kT} + \frac{\Delta\bar{S}_H^{xs}}{k} \tag{2.2.1}$$

where $\theta=N_u/N_v$, and N_u is the number of solute (dissolved hydrogen) atoms, while N_v is the number of solvent (metallic) atoms, and $\Delta\bar{H}_u^{\infty} = \overline{H_u^{\infty}} - {}^1/_2 H_{u_2}^o$ is the relative partial molar enthalpy with respect to H_2 molecules and $\Delta\bar{S}_u^{xs}$ is the relative partial excess entropy which does not vary much from metal to metal. Thus $\Delta\bar{H}_u^{\infty}$ is an effective index of the ability of a metallic system to absorb H unencumbered by hydride formation [56]. Figure 2.1 [55] summarizes the variation of $\Delta\bar{H}_u^{\infty}$ for a range of metals labeled by their Group Number in the Periodic Table.

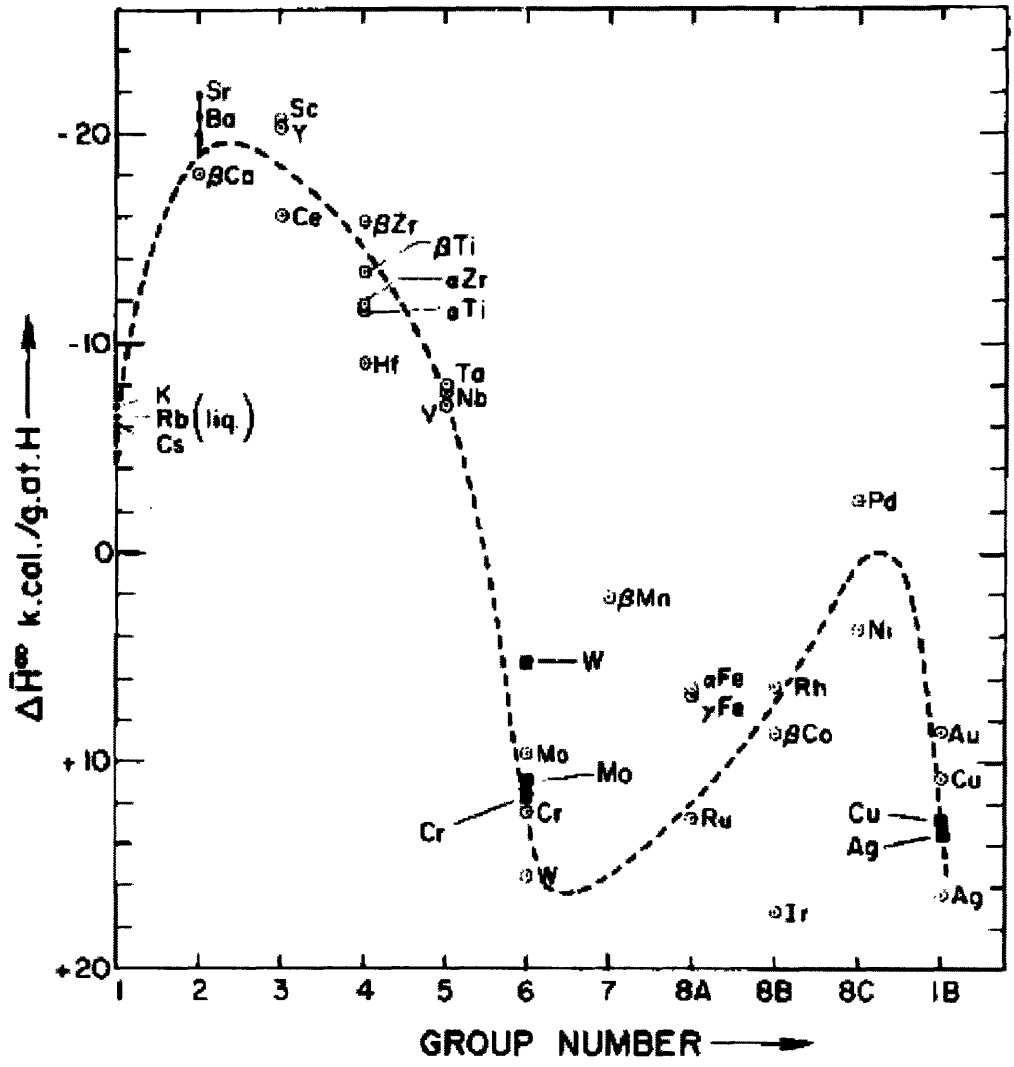

Figure 2.1. Variation of the relative partial enthalpy of solution at infinite solute dilution with the group number of solvent metal. [55]

Figure 2.1 reveals a pattern in which there is a high maximum for Group II elements which sharply falls to a minimum for the group VI and then is followed by a gentler recovery to another local maximum for group VIII metals. As McLellan points out [55], these results (with the exception of Pd) are consistent with a theory of hydrogen-transition metal bonding based on the rigid band model in which it is energetically more favorable to treat the metallic matrix as an electron acceptor and the hydrogen atom as an electron donor, even if the accepted electron must go into an anti-bonding region of the d-band for the late transition metals. From a chemical bonding standpoint, the rigid band model also suggests that electron donation from small amounts of contained hydrogen would, in principle, increase the cohesive energy and theoretical strength of the early transition metals, but decrease the cohesive strength of the late transition metals and their alloys.

Thermodynamic functions can be extracted from the solubility data by correlating thermodynamic variables with measured solubility values. For instance, in the case of equilibrium between a gas of pressure P_{u_2} and a dilute solution the solubility at a temperature T can be estimated from a statistical mechanical model to be [57]:

$$\theta = \frac{\beta {P_{u_2}}^{1/2} \lambda}{T^{7/4}} \exp\left(-\frac{\bar{H}_u - \frac{1}{2}E_D^0}{kT}\right) \exp\left(\frac{\overline{S_u^{xs}}}{k}\right) \qquad (2.2.2)$$

where $\lambda = \left(\frac{h^3}{(4\pi mk)^{\frac{3}{2}}} \frac{2h^2}{8\pi^2 Ik^2}\right)^{1/2}$ and h is Planck's constant, m is the mass of the hydrogen atom, I is the moment of inertia of the H_2 molecule, $-E_D^\circ$ is the dissociation energy per atom of the H_2 molecule at 0 K, and β is the number of sites per metallic solvent atom. So by fitting experimental solubility data we can obtain the adequate partial enthalpy and entropy; then we can approximate $\Delta\bar{H}_u$ and $\Delta\bar{S}_u^{xs}$ by [55]:

$$\Delta\bar{H}_u = \bar{H}_u - \frac{1}{2}E_D^o - \frac{7}{4}kT \tag{2.2.3}$$

$$\Delta\bar{S}_u^{xs} = \bar{S}_u^{xs} - \frac{1}{2}S_{u_2}^o \tag{2.2.4}$$

where T and $S_{u_2}^o$ refer to the mean temperature of the experimental data range. These thermodynamic functions are tabulated in the review by McLellan [55] for a variety of metals and shown in table 2.1 below.

Table 2.1. Relative partial enthalpies and entropies for various metallic solvents in dilute solutions [55]

Metal	$-\bar{H}_u$(eV/atom)	$\frac{\bar{S}_u^{xs}}{k}$	$\Delta\bar{H}_u$ (eV/atom)	$-\frac{\Delta\bar{S}_u^{xs}}{k}$
Cr	9.09	4.06	2.91	6.54
W	10.63	1.22	1.27	9.38
α-Fe	10.65	2.20	1.71	7.64
γ-U	11.65	3.24	0.47	13.76
Mo	8.72	3.37	3.16	7.24
Au	10.46	0.06	1.68	10.30
Cu	8.85	5.63	3.36	4.46
Ag	8.72	3.75	3.47	6.39
Co	9.99	5.06	2.22	5.17
γ-Fe	10.20	5.09	1.66	5.63
Ni	11.04	4.55	1.02	5.86
Rb	10.27	4.65	1.63	6.04
Ru	8.56	5.29	3.29	5.46
Ir	7.10	5.54	4.50	5.14

In high solubility metals concentrated solutions ($0.5<\theta<2$) are possible, and a different methodology is necessary to obtain the thermodynamic functions from experimental data. Results for those materials can be found in the literature [55 and references therein] but are not relevant to the case of Fe-C alloys and other iron based steels.

The statistical mechanical model resulting in equation 2.2.2 has proven consistent with experimental data for a variety of metals and for analytical measurements in iron at high

temperatures. However, permeability experiments in the range 49 to 506 °C by Quick and Johnson [58] for zone refined Ferrovac E iron with 0.026 wt pct C as the principal impurity, which have shown agreement with a variety of models and experimental measurements in the literature [10, 59, 60], are not consistent with equation 2.2.2. at lower temperatures in which the effects of the defect structure are more pronounced. The permeability results [58] show that for the reaction:

$$\frac{1}{2}H_2 \Leftrightarrow \underline{H} \tag{2.2.5}$$

where $\underline{H}$ is the hydrogen in solution, the atom fraction θ of hydrogen in equilibrium with hydrogen gas at a pressure P_{u_2}, in atmospheres, and T in K, is given by:

$$\theta = 0.00185\sqrt{P_{u_2}}\exp\left(\frac{-3440}{T}\right) \tag{2.2.6}$$

At high pressures (>2x10^7 Pa) P_{u_2} should be replaced by the fugacity f [61]. This relationship implies a constant partial enthalpy of hydrogen in iron at low temperatures of 7.32 eV/atom, which is about 3 eV/atom lower than that obtained from the statistical mechanical measurements discussed previously which include a factor of $T^{7/4}$ and effectively reduces the absolute magnitude of the entropy change in the reaction 2.2.5 biasing it toward the right-hand side. A more refined statistical mechanical model accounting for the divergence with the permeability results at low temperature can be obtained by assuming that the activation energy for hydrogen diffusion in the matrix is so low that it equals the thermal energy at 555 °C indicating that the hydrogen atom must be treated as at least partly delocalized and translating in one degree of freedom, then the average partition function for $\underline{H}$ is given by [10]:

$$Z = \left\{\frac{h^5[1-\exp(-h\nu_v/kT)]}{(2\pi mkT)^{\frac{3}{2}}(8\pi^2 IkT)}\right\}^{\frac{1}{2}} * \left\{X_L[1-\exp(-h\nu/kT)]^3 + \frac{X_D[1-\exp(-h\nu/kT)]^2\,(2\pi m^* kT)^{\frac{1}{2}}}{h}\right\}\exp(-E_o/kT)$$

(2.2.7)

where ν_v and ν are the vibrational frequencies of H_2 and H respectively, m^* is the effective mass of the delocalized H, E_o is the energy of solution at 0 K, and X_L and X_D are the fractional times that H is localized or delocalized respectively, and all other variables have been defined previously. With this refined model, the $T^{7/4}$ factor appears when the exponential containing ν_v is expanded in a Taylor series. The delocalization then decreases the entropic contribution at high temperature as well as the constant partial enthalpy therefore approximating both the results in equation 2.2.2 for high temperatures and the permeability observations summarized in equation 2.2.6 for iron at lower temperatures.

2.3. *Hydrogen Embrittlement in Steels*

The most well known effect of the presence of hydrogen in high-strength steels exposed to static tensile stress lower than the yield limit is hydrogen embrittlement, that is, delayed environmental failure which may manifest itself as hydrogen-induced cracking (HIC) of various high-strength alloys, such as the Fe-C system, or loss in tensile ductility and ductile fracture for lower-strength stainless steels and other non-ferrous alloys.

The first to suggest that hydrogen-induced brittle failures were preceded by significant local plastic deformation was Beachem in 1971 [62], and evidence from fractographic studies [63,64] seems to suggest that plastic tearing is indeed a major predecessor to HIC. Among many potential plasticity mechanisms which have been proposed to account for this "hydrogen softening" effect, two in particular have gained recent support in the literature: hydrogen enhanced localized plasticity (HELP) and a stress relaxation (creep) process induced by an increased vacancy concentration resulting from the strong interaction between vacancies and hydrogen.

The HELP mechanism is much promoted by the Mechanical Engineering group at University of Illinois at Urbana-Campaign [19-21]. They have shown that the presence of hydrogen in the form of Cottrell atmospheres around the dislocation lines will "shield" the elastic stress field of dislocations, allowing dislocations of the same sign to closer approach each other in dislocation pile-ups at various obstacles. This in turn allows more dislocation glide to occur for a given loading situation, as compared to in the absence of hydrogen. In addition, studies based on *ab initio* calculations [65, 66] have found evidence that hydrogen modifies the nature of chemical bonding in aluminum in ways which seem to lead to HELP.

Experiments upon which the HELP mechanism is based rely on detailed understanding of the fracture mechanics by analyzing at sufficiently high resolution to resolve mechanistic details. High-resolution fractography of hydrogen embrittled metals, such as Ni and Fe, show extensive plastic deformation localized along fracture surfaces [14, 70]. In addition, experiments using *in situ* TEM have also been performed in a variety of hydrogen embrittled systems [71 and references therein] confirming that the fundamental character of the fracture processes involved in hydrogen embrittlement was the same and showing that hydrogen increased the dislocation

mobility under conditions of constant stress. Specimens containing stress concentrators, such as notches and cracks, failed by ductile plastic processes at the front of the notch when stressed in vacuum. However when stressed under gaseous H_2, the extent of the plasticity in the fracture mode was more confined to regions adjacent to the fracture surface. In relatively pure specimens the fracture tended to be along slip planes and the deformation accompanying the fracture was within 1 μm of the active slip planes. In addition, cracks which had stopped propagating in vacuum under a constant external load could be started and continued to propagate by solely adding hydrogen gas to the environmental cell. Observations showed that this process was related to increased dislocation activity at the crack tip where the specimen was exposed to the gas further supporting the HELP mechanism.

On the other hand, it is known that atomic hydrogen, like carbon [27], in pure iron strongly increases the equilibrium concentration (by many orders of magnitude) of crystal point defects [67, 68] by formation of relatively stable vacancy-H pairs or higher complexes. This tends to accelerate self-diffusion processes that control various characteristics of the material, e.g. the dislocation climb mechanism, thereby allowing plastic deformation, in the form of creep or stress relaxation, to progress at stresses lower than the micro-yield (dislocation glide) limit. This "softening" mechanism is much promoted by Japanese researchers [22-26] and is supported by experimental evidence of crack propagation under a hydrogen atmosphere in which the material in front of the crack is locally softened by hydrogen allowing ductile failure to occur prior to the general yielding away from the crack tip [71].

In 2000, Jagodzinski, *et al.* [69] aimed at quantifying the HELP mechanism. They referred to a slow strain-rate test (imposed low strain-rate) of pure iron, tested at low temperature (200 K), without and in presence of hydrogen (electrolytic charging). Testing in absence of hydrogen led

to a gradual stress build-up with increased strain, while a marked stress reduction (approximately 40%) occurred during periods when hydrogen was present. Jagodzinski and co-workers found that the stress relaxation effect observed was too large to be possible to explain by the HELP mechanism. Instead they concluded that the softening effect is more likely caused by the strong hydrogen-vacancy interaction leading to an increased vacancy concentration and hydrogen enhanced dislocation climb in dipole type dislocation pile-ups. This explains, for a given applied strain, the observed stress relaxation in the system.

2.4. *Hydrogen Trapping and Blistering*

Additional mechanisms by which hydrogen degrades the mechanical properties of metals rely even more directly on the interaction and structure of hydrogen with defects present in the lattice structure. For instance, hydrogen diffusing through a metallic lattice accumulates at metallurgical imperfections or "traps" which can results from solute atoms, dislocations, particle-matrix interfaces, grain boundaries, and internal voids and cracks.

It has been established in the literature [16, 58, 59, 72], that the concentration of hydrogen in trap sites, where near saturation occurs at low temperatures, follow Fermi-Dirac statistics. For a single trap site X the appropriate reaction is [10]:

$$\underline{H} + X \Leftrightarrow H_x \tag{2.4.1}$$

with a corresponding equilibrium concentration given by the expression:

$$\frac{\theta_X}{1-\theta_X} = \frac{\theta}{1-\theta} \exp\left({}^{H_B}/_{kT}\right) \tag{2.4.2}$$

Where H_B is the binding enthalpy of the defect and normally the 1-θ term can be ignored since the hydrogen concentrations are low in most metals and in particular in iron and steels as discussed in section 2.2. The expression in 2.4.2 is only an approximation in which the entropy

of binding is assumed to be zero. This approximation is extremely accurate and entropic effects only represent a minor correction in comparison to the enthalpy of binding at the temperatures of interest. From equation 2.2.6, and assuming $\theta << 1$, we find:

$$\frac{\theta_X}{1-\theta_X} = 0.00185\sqrt{P_{u_2}} \exp\left(\frac{(H_B - H_s)}{kT}\right) \tag{2.4.3}$$

where H_S is the enthalpy of solubility given in section 2.2 and P_{u_2} is in atmospheres (and replaced by the fugacity at high pressures). For multiple sites and more complicated models for closed systems equation 2.4.2 can be adjusted to reflect constraints in the total hydrogen concentration as well as the basic components forming the traps. Details on these models as well as the energetics and concentrations of a variety of cluster-like traps are discussed in extensive detail in chapter 3.

Among the extended defects, carbide interfaces and free surfaces are experimentally observed to saturate when exposed to the equilibrium vapor pressure of hydrogen and thus would not outgas. Observations also suggest that mixed or edge dislocation cores should be marginal with respect to saturation at room temperature and that grain boundaries also saturate in open systems at room temperature [10]. Hence for temperatures below ~300 K, the extended traps dominate the adsorption of hydrogen in the material and hence hydrogen can be highly concentrated in the localized extended defects which then can display dramatic property differences with respect to a more homogeneous bulk.

When sufficient hydrogen builds up at a trap, atomic or nascent hydrogen will recombine to form molecular H_2. Accumulated molecules then nucleate a gaseous phase developing high pressures inside the material, in many instances high enough to rupture inter-atomic bonds thus forming micro-voids and, in more extreme circumstances, macroscopic blisters. The blisters then embrittle the lattice and generally degrade mechanical properties.

In addition, for alloys with relatively high solubility (such as those in the austenite phase) internal hydrogen precipitation is also possible [33]. In those cases, regions around inclusions, precipitates, and laminations become embrittled by super-saturated hydrogen which can then serve as traps for the phenomena described previously. Nucleation of hydrogen gas in these regions can cause localized brittle ruptures in the structure or "flakes" which are often evident as "fisheyes" on the brittle fracture surfaces.

2.5. Decarburization and Methane Formation in Steels

Hydrogen in steels at high temperatures is able to react with carbides present in the microstructure to form decarburized structures and methane gas which has a low diffusivity because of its size [33]. Methane bubbles form and eventually grow into fissures and cracks at grain boundaries. The combined process of decarburization, which locally reduces the yield strength from the metastably prepared hardened steel, and fissure production may provide sudden and catastrophic reductions in both strength and ductility.

2.6. Summary

In view of the complexity of hydrogen effects on the deformation and fracture behavior of metals, and despite strong evidence supporting a variety of mechanisms, no firm conclusions about the underlying detailed phenomena have yet been reached. This, in turn, highlights the importance of studying the effects of hydrogen at the most fundamental level. While there are differences in both the degree and the manifestation of the embrittlement, the same general mechanisms apply to all forms of degradation with the exception of decarburization and methane formation [10]. Thus, so-called internal and external hydrogen embrittlement are distinguished by hydrogen being present uniformly or in a gradient from the surface and by the detailed effect

of hydrogen on the defect microstructure, but are not characterized by inherently different mechanisms.

An important aspect that all of these mechanisms share is their strong dependence on the atomistic interactions between hydrogen and the lattice imperfections in the form of clusters, dislocations, grain boundaries, or surfaces. In the case of iron and steels, the properties of point-defect clusters and their interaction with hydrogen have a direct influence in the migration of species in the lattice and the formation of traps. Diffusion then controls the interaction of hydrogen with extended defects leading to crack tip embrittlement, hydrogen-induced softening, and hydrogen enhanced localized plasticity.

Chapter 3

3. Point Defect Spectrum in Fe-C-H Alloys

The interactions of hydrogen with lattice defects are important and often dominant in determining its influence on the properties of metals. However, in general, these interactions are far less understood at a fundamental level than the interaction of hydrogen with a perfect lattice structure. As discussed in chapter 2, this situation results from the variety and complexity of H-defect interactions and from the experimental and theoretical difficulties that have been encountered in their study [73].

Nonetheless, advances in the understanding of hydrogen-defect interactions have been stimulated by the profound technological impact of hydrogen embrittlement and the increase in hydrogen-containing environments in applications ranging from the microelectronics industry to aero-spatial applications. Experimental developments in microscopy, electrochemistry, and spectroscopy coupled with theoretical advances and more sophisticated computer simulations have elucidated some of the basic mechanisms of the interaction of hydrogen with defects in metals such as Fe and Al [65, 66, 74, 75]. The recent progress has also raised the prospect of using hydrogen as a probe for the study of defects within materials by taking advantage of the low-temperature mobility and high reactivity of hydrogen in a controlled manner in approaches similar to tritium desorption spectroscopy. A variety of experimental ideas have been mentioned in the literature including the use of high sensitivity tools such as secondary ion mass spectrometry, nuclear-reaction profiling and channeling, nuclear decay, and infrared and Raman spectroscopy [73 and references therein].

However, despite the decades of study and the recent progress in understanding the interactions of hydrogen with lattice imperfections a multitude of questions regarding the fundamentals of hydrogen-defect interaction still remains unanswered demonstrating a need for a detailed study of the physics that govern the atomistic effects of hydrogen in imperfect lattices.

3.1. Point Defects-Hydrogen Interactions in Metals

The vacancy is the simplest defect in metals consisting of a missing atom from the regular lattice or empty lattice site with modest peripheral relaxation. Hydrogen strongly binds to this defect in most metals as indicated in a variety of experimental and theoretical publications [73 and references therein].

Given the open-volume character of the vacancy, an attractive interaction between the defect and interstitial hydrogen in solution is expected. In particular, whenever the surface chemisorption state of H is energetically favored over interstitial solution, as is usually the case [76], the derivative of energy with respect to the metal atomic density at the solution sites is positive. Under this condition atomic H is driven to recombine with the vacancy. Moreover, the local open volume associated with the vacancy is relatively large, being almost sufficient to appear to the H atom as a free surface which strongly binds with solution hydrogen as discussed in section 2.4. As a result the binding energy between a vacancy and interstitial hydrogen tends to be large and comparable to that for H in the chemisorbed state.

The occurrence of H trapping at vacancies has been demonstrated for a number of metals by positron annihilation, a probe specifically sensitive to the presence of vacancies. In the absence of hydrogen, vacancies produced by low-temperature irradiation are observed to disappear when the temperature is raised sufficiently for the damage to heal by Frenkel pair recombination or point-defect migration to sinks such as dislocation lines and grain boundaries. This event is

generally referred to as recovery stage III in the radiation damage literature, following the onset of interstitial mobility in stage I and early microstructural evolution of defect clusters in stage II. When H is present in the lattice, H-vacancy binding reduces the effective vacancy diffusivity and delays recovery stage III providing an observable signature of the trapping reaction.

Ion-beam experiments have quantified the strength of the H-vacancy interaction and have provided information on the local atomic configuration. Typically, H is ion implanted into the metal of interest, simultaneously creating vacancies to which the H is bound. During subsequent temperature ramping, nuclear-reaction profiling is used to monitor the release of H from the trapping region, and the binding energy is extracted by fitting to solutions of appropriate transport equations or comparing with the results of computational models.

Myers *et al.* [73] summarize the experimentally inferred hydrogen-vacancy binding energies as reported in table 3.1 below. Binding energies from the positron annihilation experiments tend to be less accurate due to less detailed analyses. In Al, the lighter positive muon, commonly used as a probe for hydrogen behavior, was also observed to be trapped by vacancy defects with binding energy greater or equal that 0.4 eV [77].

Table 3.1. Binding energies of H to vacancies relative to H in solution [73]

Host Metal	**Ion-beam (eV/atom)**	**Experiments**	**Positron (eV/atom)**	**Experiments**
Al	0.52		0.53	
Fe	**0.63**		-	
Ni	0.44		0.57, 0.44	
Cu	0.42		> 0.4	
Zr	0.28		-	
Nb	-		<1.0	
Mo	1.03		1.4	
Pd	0.23		-	
Ta	0.42		<1.2	

Effective-medium theory [76] has been used to treat the H-vacancy interaction from a theoretical standpoint in simple metals, and recent calculations using density functional theory

[74, 75, 78] have also succeeded at studying the stability of H-Va defects in transition metals such as Fe. The theories confirm the qualitative insight that, in most metals, H is attracted to any defect that has an associated region of reduced electron density.

Ion-channeling analysis has been used to determine the lattice location of H trapped at vacancies in a variety of metals, including BCC V, Cr, Nb, Mo, Ta, W, and Fe, as well as FCC Al, Ni, Cu, Pd, Ag, and Pt [73 and references therein]. In all of the cases, the attached H occupies a position displaced from the vacancy center where optimum bonding is achieved which is in semi-quantitative agreement with effective-medium theory. For example, in Fe, the position deduced from channeling analysis is on a line along the (100) direction between the vacancy center and a nearest-neighbor octahedral interstitial site, and is displaced from the octahedral site toward the vacancy by δ=0.04 nm [79, 80].

Metals with large vacancy concentrations occur in radiation environments where displacement cascades are produced as in nuclear fission and fusion reactors, or particle accelerators. Since the binding energy at the vacancy can be substantially larger than the migration energy, the effects of such trapping on H transport can be large and have an influence in diffusion-dependent processes such as creep. Smaller but still appreciable vacancy concentrations are caused by quenching from elevated temperatures and cold working. Furthermore heterogeneity in the system implies that the local concentrations near surfaces, cracks, or other extended defects can be orders of magnitude larger than the bulk concentration and the defect spectrum and migration behavior can change substantially from the bulk to localized regions of the material.

In contrast to the relatively well developed picture of H-vacancy binding, not much is known about the interaction of hydrogen with self-interstitial atoms (SIA) in metals. Since interstitial

solution H is usually attracted to regions of reduced electron density and repelled where the density is increased, binding to self-interstitial only occurs in the presence of additional lattice alterations about the interstitial. Rough theoretical estimates for the binding energy in Ni, Cu, Fe, and Pd using the effective-medium approach suggest a value of approximately 0.2 eV, with the minimum-energy positions being close to the four octahedral sites about the axis of the (100) interstitial dumbbell [81]. Even though SIAs are statistically negligible under most non-irradiated environments, understanding of the hydrogen-SIA interactions provides an important starting point in studying the interactions with dislocations, grain boundaries, and impurity or alloying-element interstitials.

The interaction of H with impurities/solutes in metals is influenced by the elastic strain field of the lattice structure due to size differences and by the electronic disparities in H bonding with the solute and host metal. The resulting behavior is therefore substantially more complicated than that in pure metals and is responsible for the myriad of effects in industrially relevant alloys. Theoretical estimates of the two contributions to the binding have been made in a semi-empirical manner making use of phonon frequencies and some of the measured H-solute binding energies [82-84]. These calculations suggest that the primary contribution to the binding is due to the elastic strain field in the case of interstitial solutes such as N and O. For substitutional, transition-metal solutes there is a comparable contribution from the electronic effects with the degree of attraction increasing with the size of the solute and its number of d electrons.

Experimental information on the binding energies of H-solute pairs is available from a variety of methods including Mössbauer spectroscopy, perturbed angular correlation, inelastic neutron scattering, desorption, and ion-beam experiments. Some results [10,73] are summarized in table 3.2 below.

Table 3.2. Experimental H-solute binding energies in metals relative to H in solution [73]. Multiple values correspond to different references.

	System	Binding Energy (eV/atom)
Substitutional	Ti in V	0.15, 0.03-0.10
	Ti in Fe	0.19
	Ti in Ni	0.05-0.1
	Fe in Ni	0.07-0.12
	Co in Cu	0.12
	Cr in Nb	0.105
	Ti in Nb	>0.120
	V in Nb	0.09
Interstitial	C, N in V	0.13
	O in V	0.09
	C in Fe	**0.03**
	N in Fe	>0.13
	N in Nb	0.12, 0.1
	O in Nb	0.09
	N in Ta	0.06
Solute-vacancy complex	Co in Cu	0.63
	In in Ni	-0.6
	Y in Fe	0.7-0.9
	Cs in Ni	0.6-0.8

As can be observed, the binding energies for solute-hydrogen complexes are modest in the absence of vacancies or any additional distortion consistently with our expectations described in the case of the H-SIA interaction. Since the open volumes produced by lattice strain about substitutional and interstitial impurities are much smaller than the volume of the vacancy, a correspondingly reduced effect on the binding energy relative to the hydrogen in solution is to be expected. An important point is that although hydrogen binds strongly with metals (~ 2 eV as seen from the heats of chemisorptions and solution [76]), the differences in bonding which are responsible for trapping at impurities are much smaller.

Despite a good amount of experimental literature, first-principles theoretical calculations on the interactions of hydrogen with solute atoms are extremely scarce and a good understanding of the binding of hydrogen to these defects is not yet available. However, such calculations are of paramount importance since the majority of concerns of hydrogen embrittlement and hydrogen

storage revolve around the failure of metallic alloys rather than pure metals, and because the use of alloying additions is one of the most accessible means of modifying hydrogen behavior. For example, the use of appropriate alloying elements may inhibit detrimental effects of hydrogen on dislocations or grain boundaries.

3.2. DFT Calculations of Defect Binding and Stability

From a technological perspective, and as discussed in the previous section, the study of H-solute interactions and of the distributions of defect clusters is essential in understanding the phenomena of hydrogen embrittlement of metallic alloys, and more specifically of steels. Furthermore, the use of density functional theory (DFT) [85-87] has been extremely successful in providing insight on the defect structure, energetics [88-90], and concentration [27] in Fe-alloys (specifically Fe-C steels), as well as in understanding the interactions of hydrogen with point-defects in Fe as well as other metals [65, 66, 74, 75]. Therefore, it is natural to resort to the DFT calculations to address some of the unanswered fundamental questions about the stability and structure of point-defect clusters when hydrogen is introduced in a metallic system of industrial relevance such as Fe-C, which is the approach taken in this thesis.

The necessity for a quantum mechanical description of interstitial hydrogen in metals has been demonstrated by neutron scattering observations of discrete energy levels and an extended density distribution [91] which have been successfully explained through quantum-mechanical calculations [92-95]. Motivated by past studies [27, 88-90] described above we have performed DFT [85-87] total energy calculations in a matrix of bcc Fe studying various configurations and combinations of C, H, and vacancy clusters. As has been discussed in previous sections, the Fe-C-H system has immense technological relevance as it is an idealized, but realistic, representation of hydrogen exposed hardened steels. The total energy DFT calculations were

performed using the VASP code [96, 97] with Blöchl's projector augmented method [98, 99]. All the calculations were carried out with a plane-wave energy cutoff of 400 eV in 128-atom super-cells with the theoretical lattice constant of 2.835 A, using a 2x2x2 k-point mesh for integration over the Brillouin zone and a Methfessel Paxton Fermi-surface smearing parameter of 0.05 eV [100]. The calculations included spin polarization effects and were started from a ferromagnetic charge density. No symmetry constraints were imposed. The geometry relaxation was terminated with a force cutoff of 5 meV/A.

The first qualitative finding of our study is that the energy landscape of the Fe(bcc)-C-H-vacancy point-defect system is extremely complex and possesses numerous shallow local minima near the optimized geometry for a given defect stoichiometry. Thus a variety of geometric configurations must be explored to relaxation to find the true global energy minima for the configurations. This in turn implies that our results for the binding energies of the defect complexes are only accurate to within 0.1-0.2 eV which corresponds to the characteristic energy variation of wells surrounding an optimized geometry.

Nevertheless, despite the uncertainty associated with our results we can still obtain conclusive information regarding the relative stability of the different defect species, which in turn will determine the relative concentrations as is discussed in the following sections.

We define the formation energy of a point-defect complex in a closed system as follows:

$$E_{form}(n_V, n_H, n_C) = e(n_V, n_H, n_C) - \frac{N-n_V}{N} * e_{perfect} - n_H * e_H - n_C * e_C \qquad (3.2.1)$$

where n_V, n_C, and n_H are the number of vacancies, carbon atoms, and hydrogen atoms in the cluster, respectively. N is the total number of lattice sites in the simulation (128 in our case), $e(n_V, n_H, n_C)$ is the calculated DFT energy for the bcc matrix with one of the desired defect clusters, and $e_{perfect}$, e_H, and e_C representing the DFT energies of the perfect bcc Fe lattice, and

free hydrogen and carbon atoms in vacuum respectively. Using equation 3.2.1 in combination with our DFT results we find that the formation energy for a carbon octahedral interstitial is 0.58 eV -- 0.86 eV lower than that for a C tetrahedral interstitial and therefore consistent with experimental observations [28] which predict that C sits on octahedral sites. In contrast, atomic hydrogen is more stable as a tetrahedral interstitial with calculated formation energy of -2.06 eV (compared to -1.93 eV for the octahedral sites), which again is consistent with empirical data [101]. Our calculated heat of solution for hydrogen in tetrahedral positions of 0.19 eV is also consistent (within the uncertainty previously described) with the experimental value of 0.30 eV [10].

At a temperature of 160 °C, where the body-centered tetragonal phase transforms to bcc in hardened metastable Fe-C alloys, the vibrational free-energy contribution at most amounts to 0.2 eV at the temperature of interest [27], which is within the margin of error in our predictions and hence neglected. Table 3.3 then summarizes our complete formation energies as calculated from equation 3.2.1.

Table 3.3. Calculated formation energies for different defect stoichiometries. Only the deepest energy minima for each defect stoichiometry is shown.

Defect Species	**E_{form} (eV)**	**Defect Species**	**E_{form} (eV)**
$H_{tetrahedral}$	-2.06	1H+1C+2Va[100]	1.19
$C_{octahedral}$	0.58	1H+1C+2Va[111]	1.70
Va	2.01	1H+2C+1Va	-0.26
2Va[100][a]	3.87	1H+2C+2Va[100]	1.60
2Va[111]	3.90	1H+2C+2Va[111]	0.75
1H+1Va	-0.56	2H+1Va	-3.09
1H+2Va[100]	1.21	2H+2Va[100]	-1.31
1H+2Va[111]	1.28	2H+2Va[111]	-1.38
1C+1Va	2.07	2H+1C	-3.50
1C+2Va[100]	3.58	2H+1C+1Va	-2.44
1C+2Va[111]	3.83	2H+1C+2Va[100]	-1.28
1H+1C	-1.50	2H+1C+2Va[111]	-0.82
$2H = H_2$	-4.13[b]	2C+2Va[100]	3.38
1H+1C+1Va	-0.60	2C+2Va[111]	3.29

[a][...] represents the iron vacancy dumbbell direction.

[b]Note that the formation energy of molecular hydrogen is extremely low since we define our formation energy in 3.2.1 with respect to free atomic rather than free molecular hydrogen.

The associated geometrical configurations for some key clusters are shown below in figure 3.1 as well:

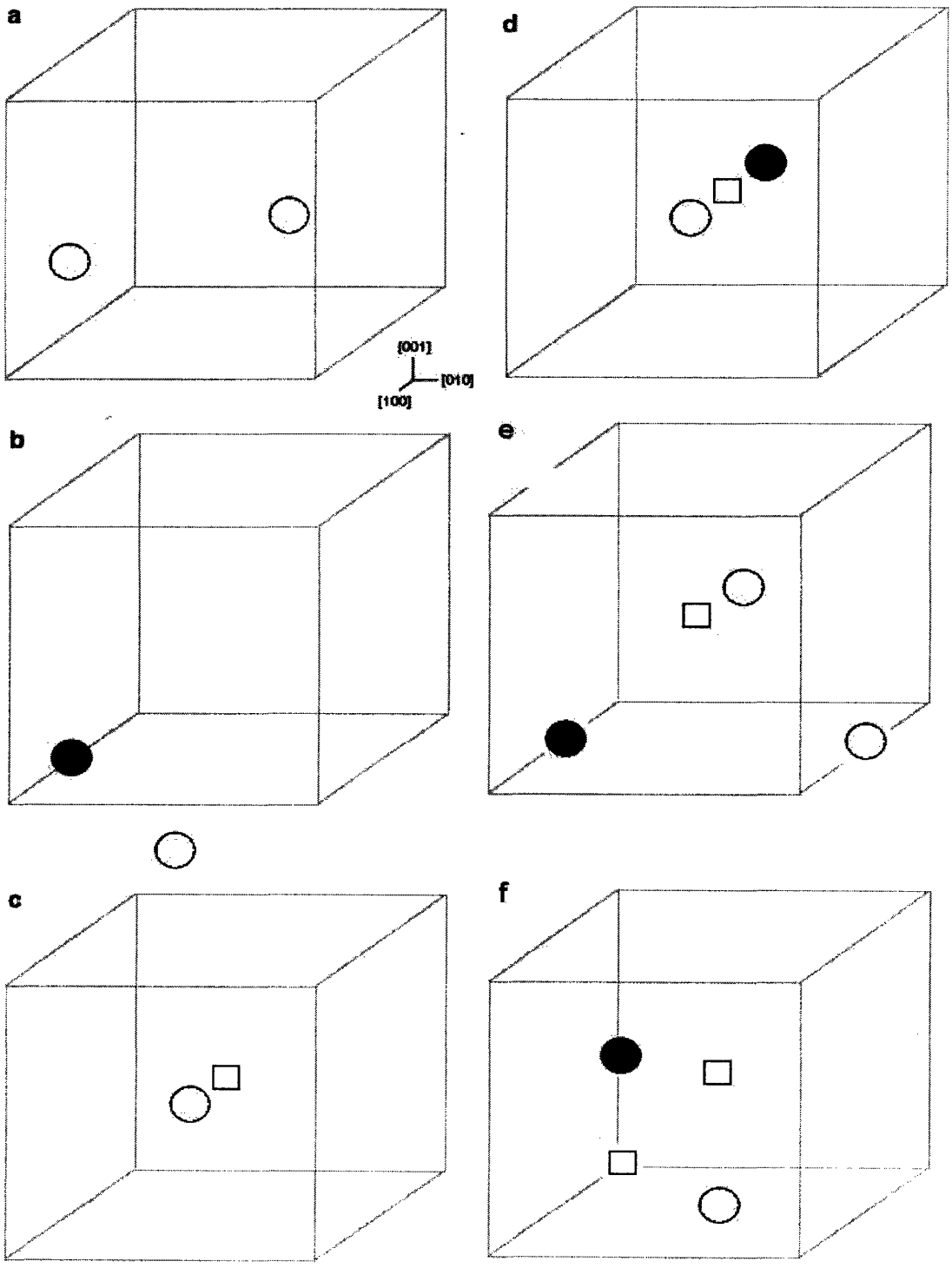

Figure 3.1. Schematic of the approximate locations of the atoms in the configurations corresponding to key defect complexes. (a) the H_2 molecule of 2 H atoms in adjacent tetrahedal positions of (a/2, 0, a/4) and (0, a/2, a/4); (b) the 1C-1H cluster of the C atom in (a/2, 0, 0) and the H atom in (3a/2, 3a/4, 0); (c) the 1H-1Va <100> cluster of the vacancy at (a/2, a/2, a/2) and the H atom at (a, a/2, a/2); (d) the 1H-1C-1Va <100> cluster of the vacancy at (a/2, a/2, a/2), the C atom at (0, a/2, a/2), and the H atom at (a, a/2, a/2); (e) the 2H-1C-1Va cluster of the vacancy at (a/2, a/2, a/2), the C atom at (a/2, 0, 0), and the H atoms at (0, a/2, a/2) and (a/2, a, a/2); and (f) the 1H-1C-2Va<111> cluster of the vacancies at (0, 0, 0) and (a/2, a/2, a/2), the C atom at (0, 0, a/2) and the H atom at (a/2, a/2, 0). C atoms are drawn in solid circles, H atoms are drawn in empty circles, and Fe atoms are not shown.

In order to compare the results of our calculations in table 3.3 with experimental values of the binding energies, we consider the cluster formation energies relative to the lowest energy constituent defects, i.e. monovacancies, octahedral carbon interstitials, and tetrahedral hydrogen interstitials. Table 3.4 summarizes the binding energies of various clusters given by:

$$E_{binding}(n_V, n_H, n_C) = n_V * E_{form}(n_V = 1, n_H = 0, n_C = 0) + n_H * E_{form}(n_V = 0, n_H = 1, n_C = 0) + n_C * E_{form}(n_V = 0, n_H = 0, n_C = 1) - E_{form}(n_V, n_H, n_C) \quad (3.2.2)$$

Table 3.4. Calculated binding energies for different defect stoichiometries. Only the deepest energy minima for each defect stoichiometry is shown. Experimental values are given in parenthesis for comparison where available.

Defect Species	$E_{binding}$ (eV)	Defect Species	$E_{binding}$ (eV)
$H_{octahedral}$	-0.12 (-0.07 [Ref. 101])	1H+1C+2Va[100]	1.37
$C_{tetrahedral}$	-0.86	1H+1C+2Va[111]	0.87
2Va[100]	0.17	1H+2C+2Va[100]	1.53
2Va[111]	0.14	1H+2C+2Va[111]	2.39
1H+1Va	0.52 (0.46 [Ref. 7])	2H+1Va	0.98
1H+2Va[100]	0.76	2H+2Va[100]	1.22
1H+2Va[111]	0.70	2H+2Va[111]	1.29
1C+1Va	0.53 (0.85 [Ref. 28])	2H+1C	-0.05
1C+2Va[100]	1.04	2H+1C+1Va	0.92
1C+2Va[111]	0.79	2H+1C+2Va[100]	1.77
1H+1C	0.02 (0.03 [Ref. 102])	2H+1C+2Va[111]	1.31
$2H = H_2$	0.01 (0.04 [Ref. 102])	2C+2Va[100]	1.04
1H+1C+1Va	1.14	2C+2Va[111]	0.79
1H+2C+1Va	1.38		

From the binding energy values in table 3.4 we notice that H-C complexes do not form (within our uncertainty range) in the absence of vacancies. This is again consistent with our

physical picture in which hydrogen is repelled by areas with increased mass and electron density, as well as with experimental observations and other theoretical calculations discussed in section 3.1. In addition we observe that both H-Va and C-Va clusters are sufficiently stable in our temperature range, and as such we expect that both impurities will stabilize the free vacancies and increase the effective vacancy concentration in the materials. This is in fact the case as is explained in more detail in the following sections dealing with the spectrum of the point-defect clusters.

In addition by comparing the binding energies for the sets {1H+1Va, 1C+1Va, 1H+1C, 2H+1Va, 2C+1Va, 1H+1C+1Va} and {2H+2Va, 2C+2Va, 1H+1C+2Va} we notice that hydrogen is unable to displace carbon atoms from pure C-Va complexes after they are formed (i.e. if for example the hydrogen impurity is added after the metastable Fe-C is formed), but rather tends to bind to existing C-Va clusters or form separate H-Va complexes. However, the complete spectrum is strongly dependent on the detailed local concentrations of C, H, and free vacancies in a closed system or alternatively on the corresponding chemical potentials for an open system.

Another observation from table 3.4 is that the hydrogen molecule and interstitial hydrogen in solution are in close thermodynamic equilibrium at our temperatures of interest. However, given the uncertainty of ~0.2 eV in our energies only a semi-qualitative description of this equilibrium is appropriate. Nevertheless, the results show that since the energy of formation of the hydrogen molecule in the Fe matrix is not very high, high H-pressure environments should induce molecular hydrogen formation which can then congregate into larger clusters forming gaseous hydrogen bubbles and blisters. The details regarding the recombination of atomic hydrogen into

hydrogen molecules in different types of complexes as a function of the hydrogen pressure and other environmental variables is discussed in more detail in section 3.5.

3.3. *Point-Defect Clusters in Fe-C Alloys*

Först [27] studied the cluster spectrum in metastable Fe-C alloys at 160 °C using similar *ab initio* total energy calculations and then computed the defect concentrations by using a statistical mechanical model based on the minimization of the overall Helmholtz free energy with respect to defect formation with constrained total carbon and vacancy concentrations. However, as pointed by Lau [31] there are several defects with Först's statistical model stemming from the fact that the defect concentration is not rigorously defined and an incorrect interpretation of the configurational entropy is used.

Following Lau's [31] approach we proceed by rigorously defining the defect concentration in the defect sub-lattice as:

$$[defect_{sub-lattice}] = \frac{number_{defect}}{number_{bcc\ lattice\ positions}} \tag{3.3.1}$$

As discussed in chapter 2 and section 3.1, in Fe-C the entropic contributions are small relative to the binding enthalpies. Thus, for the purposes of obtaining the relative defect populations, our total-energy calculations from section 3.2 provide an accurate approximation for the full binding energies. In addition, if we assume defect species are ideal and both carbon and iron behave classically given the temperatures of interest, the concentration of each defect species can be expressed as:

$$[xVa - yC] = [Va_{BCC}]^x [C_{oct}]^y \exp\left(\frac{E_{binding}(n_V=x, n_C=y)}{kT}\right) \tag{3.3.2}$$

Then for a closed system we can define the following constraints:

$$[Va_{tot}] = \sum_{clusters} x * [xVa - yC] \tag{3.3.3}$$

$$[C_{tot}] = \Sigma_{clusters}\, y * [xVa - yC] \quad (3.3.4)$$

Using equations 3.3.2-3.3.4, we can then calculate the defect concentrations for the Fe-C system with no hydrogen. Figure 3.2 shows a plot for the case in which $[C_{tot}]$=0.01, corresponding to a steel with 1.0 at % C.

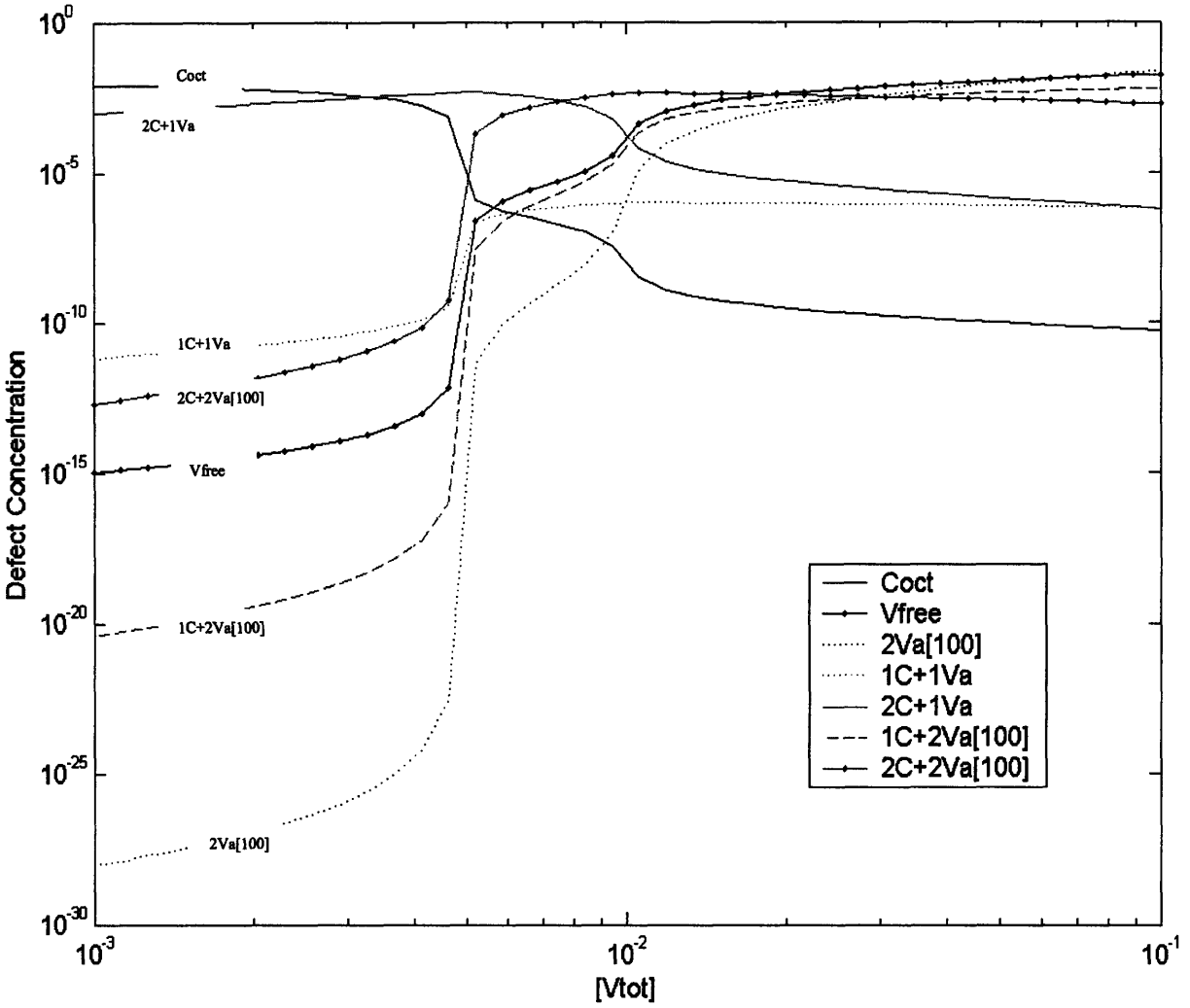

Figure 3.2. Partial point-defect cluster spectrum in Fe-C alloys as a function of total vacancy concentration for $[C_{tot}]$=0.01. For defects with identical composition only the most statistically significant one is shown. Larger clusters with different stoichiometry are not shown.

We notice that, as predicted from energetic considerations, the concentrations of 1C+1Va, 2C+1Va, and 2C+2Va defects are much higher than that of free vacancies at total vacancy concentrations below 0.01. This implies that carbon binds with vacancies and stabilized them in the form of multi carbon-vacancy clusters and thus the total stable vacancy concentration

can be orders of magnitude higher than that for a pure Fe matrix, once again consistent with previous work by both Först [27] and Lau [31].

In addition we find that the predominant defect clusters vary from octahedral carbon interstitials at low vacancy concentrations, to 2C+1Va clusters in the range of vacancy concentrations from 0.2 at. % to approximately 0.8 at. %. At higher concentrations di-vacancy clusters become more prevalent and bind to carbon changing the prevalent stoichiometry to 2C+2Va defects. Other defects remain statistically significant throughout the complete range of total vacancy concentrations as well.

Finally we observe that at a "critical" or threshold vacancy concentration of approximately 0.5 at. % the concentrations of a variety of defect clusters sharply increase several orders of magnitude reflecting extremely non-linear behavior. The drastic change in the defect spectrum as a result of the critical changes shows that local changes in vacancy concentration can have an extremely pronounced effect in the local point-defect microstructure. This in turn implies that the diffusive behavior, which is controlled by the migration of the statistically significant defects, can in principle change dramatically with only small changes in the vacancy concentration. This critical behavior and the underlying relation with the topology of the energy landscape will be discussed in more detail in the following section.

In summary, the results shown in figure 3.2 indicate that even in for meta-stable Fe-C with no hydrogen the point-defect microstructure is extremely complicated and a variety of defects are statistically significant throughout a wide range of vacancy concentrations. Hence we expect that, in principle, the diffusion processes in the material are controlled by different migration barriers for each of the species and diffusion-dependent processes such as creep and other forms of structural relaxation will be correlated to the detailed changes in the defect

spectrum. Nonetheless, there is also the possibility of very different migration barriers for the statistically significant defect complexes, in which case the diffusion behavior would be dominated by a single defect species. Computational methodologies to quantify the true behavior and link the results of this thesis to the larger-scale phenomena that characterize embrittlement are discussed in chapter 4.

3.4. Critical Behavior and Activated Processes

One characteristic feature in figure 3.2 is the sharp increase in the concentrations of the 2Va[100], 2C+1Va, 1C+2Va[100], and 2C+2Va[100] defect clusters at a total vacancy concentration of approximately 0.005 = 0.5 at. %. Examples of similar critical threshold behavior are present in a variety of physical systems ranging from the heat capacity of solids at low temperatures to the viscosity of super-cooled liquids.

The underlying mechanism behind many of the phenomena which show threshold behavior consists of an activated process in which an activation barrier prevents the system from reaching a particular state unless enough energy is available. In analogy to those cases we define an environment-dependent effective activation energy barrier for the formation of each type of defect cluster as:

$$\Delta E^{eff}_{activation}(n_V = x, n_C = y) \equiv \log\left(\frac{[xVa\text{-}yC]}{[V_{tot}]^x[C_{tot}]^y}\right) \qquad (3.4.1)$$

For the component defects (free vacancies and octahedral carbon interstitials), $\Delta E^{eff}_{activation}$ represents exactly the energy required for formation in the presence of other defects compared to that in which only the defect in question is present, i.e. it includes environment-effects related to the possible presence of alternative defect complexes. For larger defects the effective activation barrier as defined above has the same physical meaning only approximately and becomes exact

in the limit of small V_{tot} and C_{tot}. However, we find that the effective barrier, as defined in equation 3.41, approximately describes the energy space topology of the system and provides an appropriate measure to discuss the energy landscape.

Figure 3.3 below shows the calculated effective barriers using 3.4.1 corresponding to the defects shown in figure 3.2.

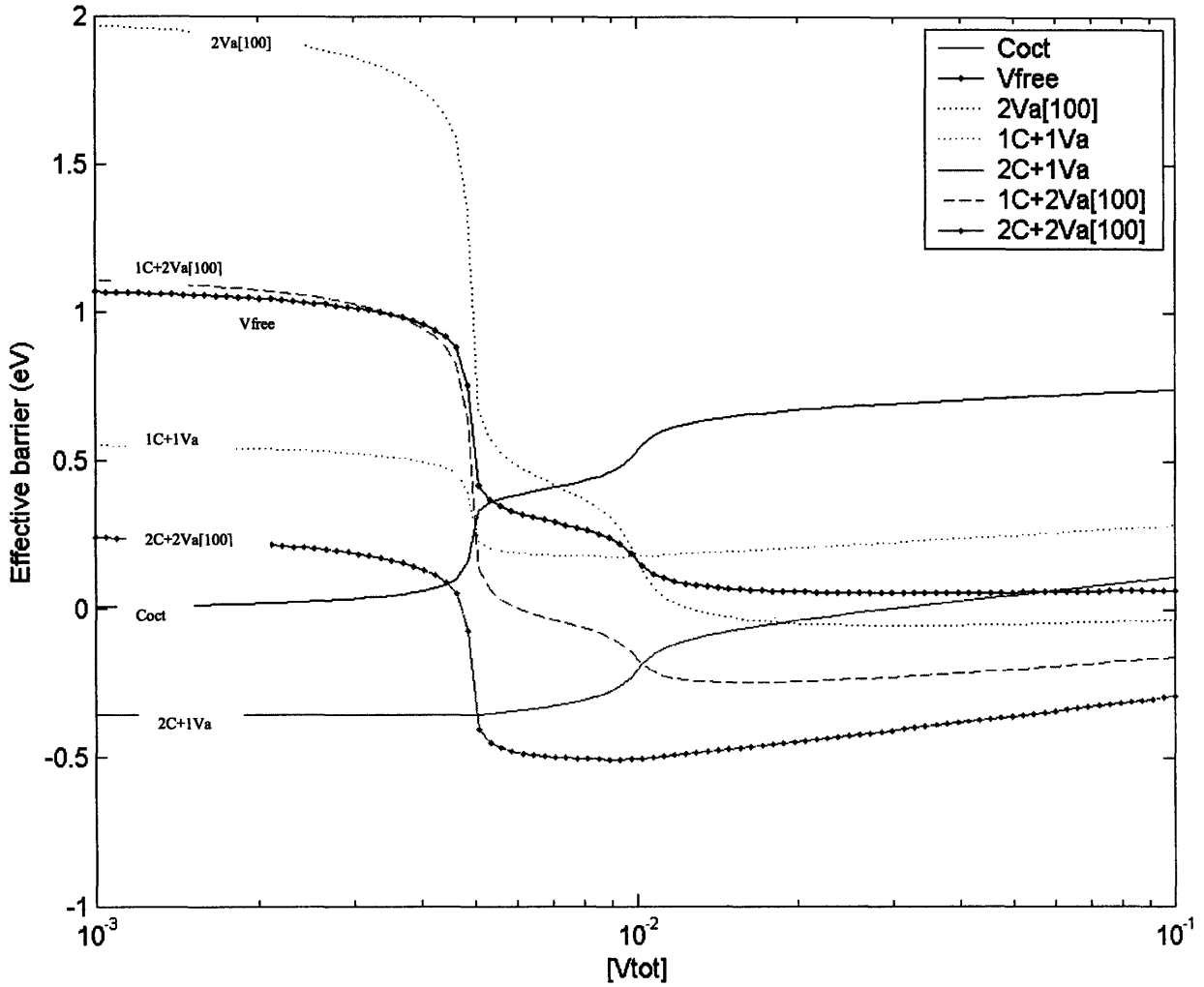

Figure 3.3. Effective activation barriers for key point-defect clusters in Fe-C as a function of total vacancy concentration for $[C_{tot}]$=0.01.

We notice from figure 3.3 that the effective barriers for the defects drastically change as we vary the total vacancy concentration which in principle can be linked to the system moving to different wells in the energy landscape. Negative barriers in the figure correspond to defect

clusters which are thermodynamically favored in comparison to alternative complexes, and could be interpreted as "peaks" or "plateaus" in the energy landscape.

In addition, at very low vacancy concentrations the effective activation barrier for octahedral carbon interstitials is 0 eV implying that in the absence of vacancies carbon will preferentially remain as interstitials in solution. On the other hand, at high vacancy concentrations the prevalent defect also (2Va[100]) approaches an effective barrier of approximately 0 eV. However it captures a similar physical picture to the low vacancy concentration regime only in a semi-quantitative way due to the approximations made in interpreting equation 3.4.1.

Through this activation approach we can then link results about the point-defect spectrum directly with the topology of the free energy landscape as a function of chemical composition of the alloy. Then, by analogy with the modeling of the viscosity of super-cooled liquids we can then use energy landscape sampling techniques to obtain information about the detailed critical behavior of the system as well as the nature of the point-defect cluster concentrations, thereby linking observables to the fundamental energetic and thermodynamic properties of the system.

3.5. *Effects of Hydrogen in the Fe-C Spectrum*

The inclusion of hydrogen into the Fe-C systems can be accounted for in a straight-forward manner by generalizing equations 3.3.2 – 3.3.4 to:

$$[xVa - yC - zH] = [Va_{BCC}]^x[C_{oct}]^y[\mathrm{H_{tet}}]^z \exp\left(\frac{E_{binding}(n_V=x, n_C=y, n_H=z)}{kT}\right) \quad (3.5.1)$$

$$[Va_{tot}] = \sum_{clusters} x * [xVa - yC - zH] \quad (3.5.2)$$

$$[C_{tot}] = \sum_{clusters} y * [xVa - yC - zH] \quad (3.5.3)$$

$$[H_{tot}] = \sum_{clusters} z * [xVa - yC - zH] \quad (3.5.4)$$

The trivial generalization assumes bosonic statistics for hydrogen in contrast with the observations mentioned in section 2. This approximation is valid because of the high temperatures of interest (160 °C) as well as the low concentrations of hydrogen and of hydrogen-containing defects which assure that $\frac{c}{1-c} \approx c$, where c is the concentration of the defect. For lower temperatures or higher hydrogen concentrations in which the Fermi-Dirac statistics become more important we can replace $[H_{tet}]$ by $\frac{[H_{tet}]}{(1-[H_{tet}])}$.

From equations 3.5.1-3.5.4 we then find the changes in the point-defect spectrum by the introduction of hydrogen which are summarized in figures 3.4-3.8 below:

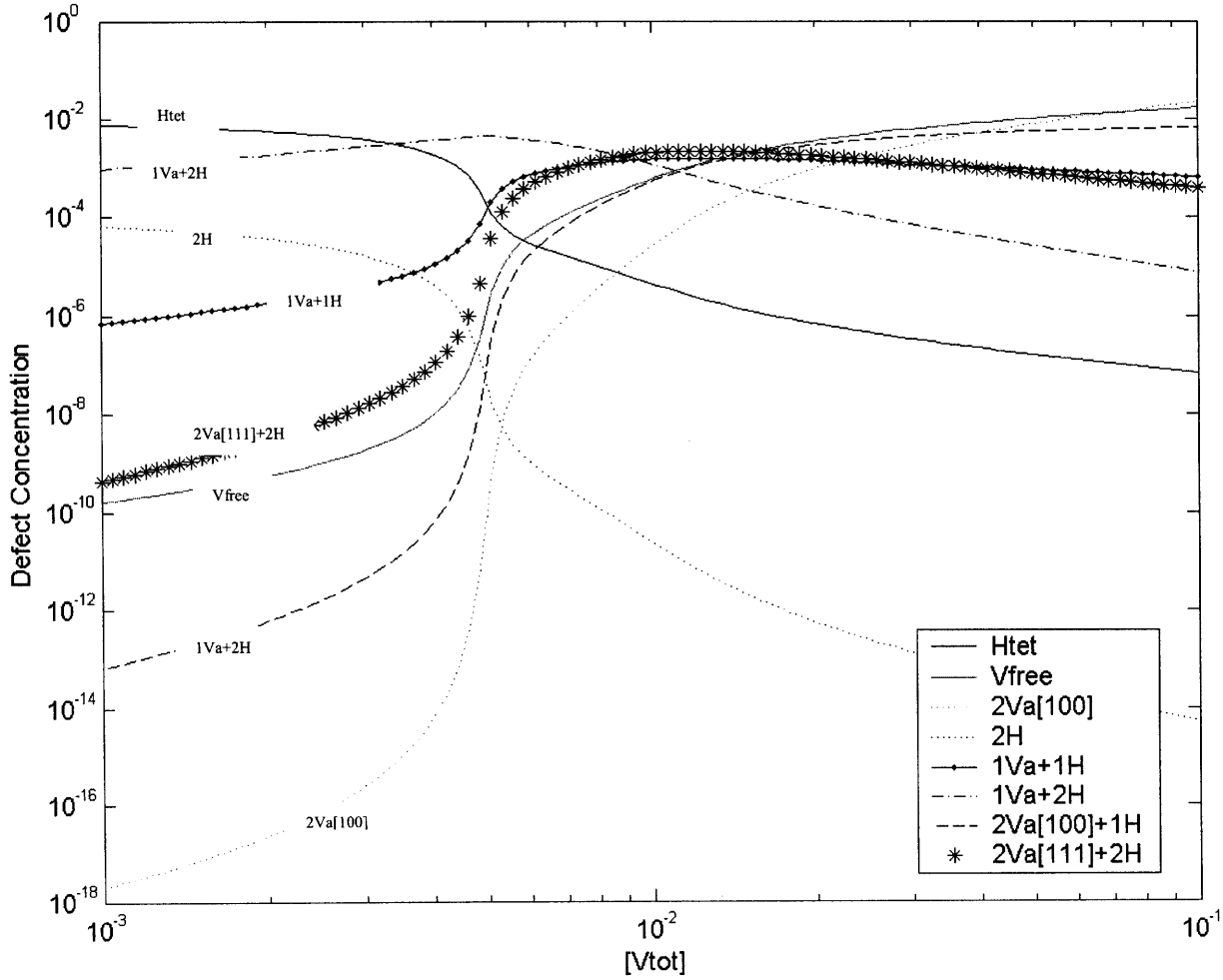

Figure 3.4. Partial point-defect cluster spectrum in Fe-H alloys as a function of total vacancy concentration for $[H_{tot}]$=0.01. For defects with identical composition only the most statistically significant one is shown. Larger clusters with different stoichiometry are not shown.

Figure 3.4 shows the point-defect cluster of pure Fe with hydrogen impurities (i.e. the Fe-H system with no C). Once again we notice some of the same features observed in figure 3.2 for carbon such as the sharp critical behavior, though in the case of hydrogen the criticality is less pronounced due to the weaker binding between hydrogen and vacancies in compared to carbon as is observed in table 3.2. This indicates that the free energy landscape topology is "smoother" with shallower and less steep wells for weaker binding, and as such we expect that additional alloying elements such as Cr or Mn will sharpen or smooth the thresholds depending on the strength with which they bind to the vacancies.

Again we see that for a wide range of low total vacancy concentrations the 1Va+1H, 1Va+2H, and 2Va+2H defects have much higher concentrations than the free and di-vacancies. Hence we expect that hydrogen will stabilize free vacancies in iron and thus increase the vacancy content in the material. Finally, and similarly to carbon, the prevalent defect stoichiometry of the defects switches from 1Va-2H to 1Va-1H (2Va-2H) to 2Va-1H with increasing total vacancy concentration.

In addition, we observe that interstitial atomic hydrogen is prevalent over molecular hydrogen in the constrained geometries of the Fe BCC lattice in the absence of vacancies. However, in the neighborhood of a vacancy the free volume available is enough for atomic hydrogen to recombine into molecular H_2, and thus the most common defect clusters when the total vacancy concentration surpasses 0.3 at. % contain H_2 rather than atomic hydrogen.

By adding carbon to the system, we then obtain a simplified model of hardened steels exposed to hydrogen pressures. For an alloy with $[C_{tot}]=0.01$ (1 at. %) and $[H_{tot}]=0.001$ (0.1 at. %, 10^3 ppm) this corresponds to a hydrogen pressure of 2.32 MPa= 23.2 atm at 160 ℃, according to equation 2.2.6. However, temperature changes during operation or manufacturing

can allow the hydrogen content to increase at much lower pressures. For instance, at 1700 K (~180 K below the melting temperature of Fe) the necessary hydrogen pressure to produce $[H_{tot}]=10^3$ ppm = 0.001 is just 16.7 Pa = 1.67×10^{-3} atm, which is close to the atmospheric water vapor pressure close to the surface and possibly attainable in poorly evacuated facilities. For T=200 °C and T=300 °C the necessary hydrogen pressures are 6.06 atm and 0.48 atm, respectively. Figure 3.5 summarizes this low hydrogen content case:

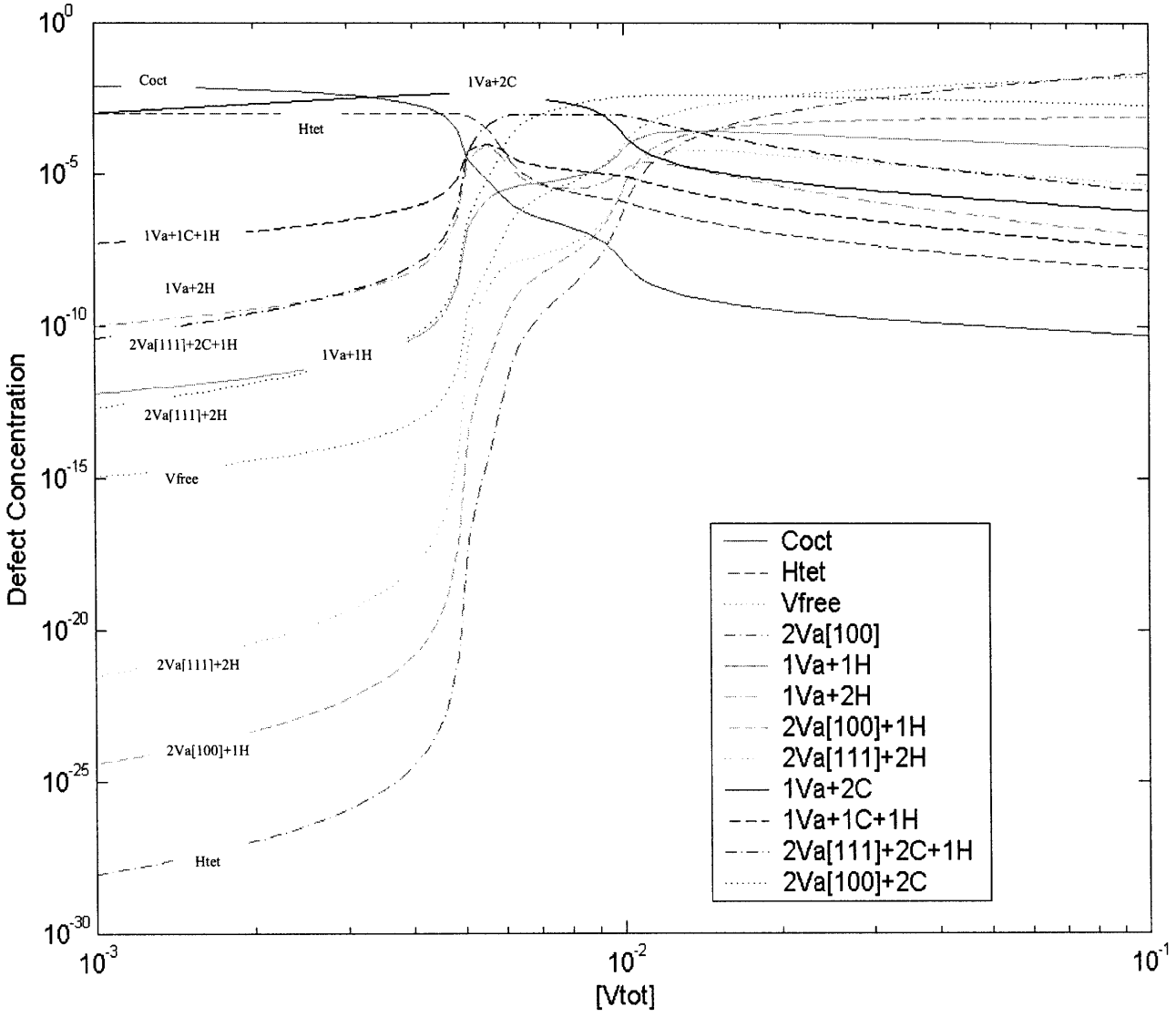

Figure 3.5a. Partial point-defect cluster spectrum in Fe-C-H alloys as a function of total vacancy concentration for $[C_{tot}]=0.01$ and $[H_{tot}]=0.001$. For defects with identical composition only the most statistically significant one is shown. Larger clusters with different stoichiometry, and defects with low concentrations throughout the range of V_{tot} are not shown.

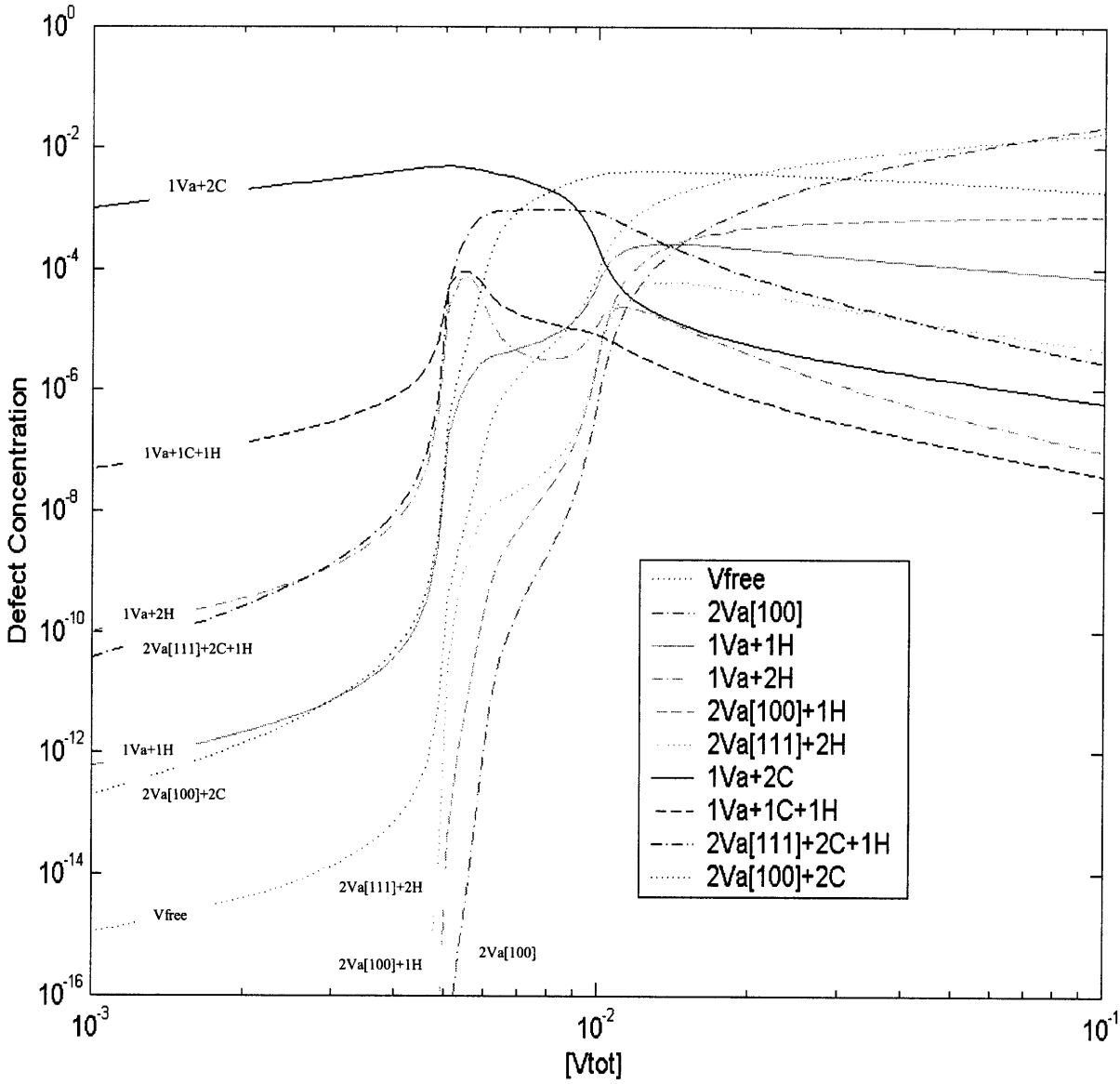

Figure 3.5b. Partial point-defect cluster spectrum in Fe-C-H alloys as a function of total vacancy concentration for $[C_{tot}]=0.01$ and $[H_{tot}]=0.001$. For defects with identical composition only the most statistically significant one is shown. (Magnified version of 3.5.a with C_{oct} and H_{tet} defects not shown for clarity)

In contrast to the simple curves in figures 3.2 and 3.4 we see that the spectrum in a ternary system shown in figures 3.5a and 3.5b is vastly more complex than that for only one alloying element. Although the most common defects (C_{oct}, 1Va-2C, 2Va-2C) remain the same as in the case with no hydrogen (figure 3.2), the detailed spectrum is much more complex and the number of statistically significant defects (within 2 or 3 orders of magnitude from the main defect) is substantially larger. In particular, in the case of low hydrogen content shown in figure 3.5, we

see that for total vacancy concentrations from 0.007 to ~0.01 the 1Va-1C-1H defect is a main contributor with a concentration within the same order of magnitude as 1Va-2C and 2Va-2C, and as such we expect that its migration will be a main contributor to diffusive processes. Furthermore, given hydrogen's high mobility we expect that the 1Va-1C-1H defect will migrate faster than 1Va-2C and 2Va-2C clusters, and this in turn could increase the rate of dislocation climb and alter the material's creep susceptibility. At higher vacancy concentrations defect complexes such as 1Va-1H, 2Va-1H, and 2Va-2H become statistically significant. We expect that these defect clusters will have very small migration barriers, such that at small concentrations they may have an observable effect on the diffusivity.

By increasing the hydrogen pressure or raising the temperature of the system we can increase the concentration of hydrogen. If the hydrogen pressure is increased such that the H-content becomes comparable to the carbon concentration (e.g.$[H_{tot}]$=10 ppm=0.01, $[C_{tot}]$=0.01) the overall defect populations change as shown in figures 3.6a and 3.6b below:

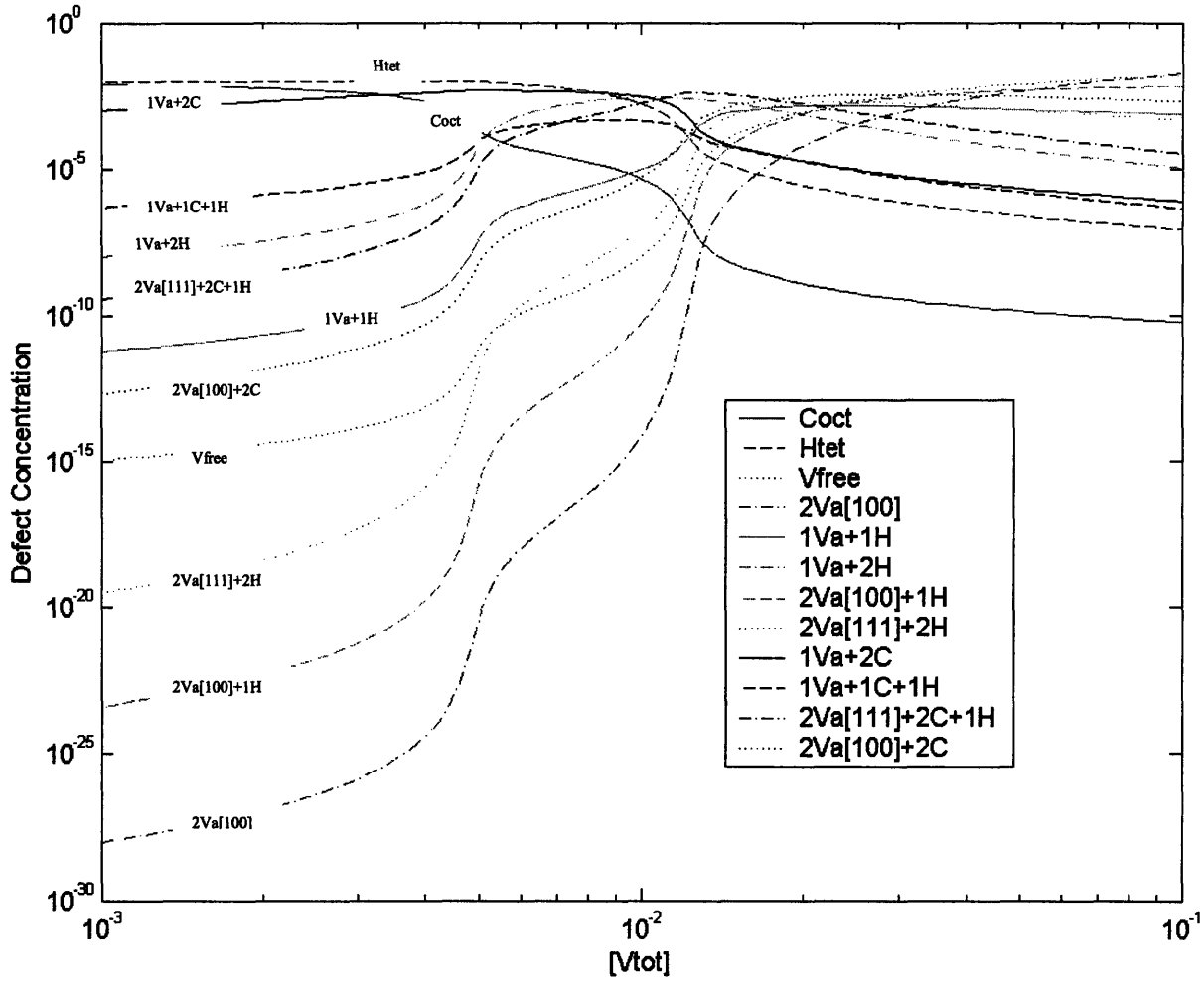

Figure 3.6a. Partial point-defect cluster spectrum in Fe-C-H alloys as a function of total vacancy concentration for $[C_{tot}]=0.01$ and $[H_{tot}]=0.01$. For defects with identical composition only the most statistically significant one is shown. Larger clusters with different stoichiometry, and defects with low concentrations throughout the range of V_{tot} are not shown.

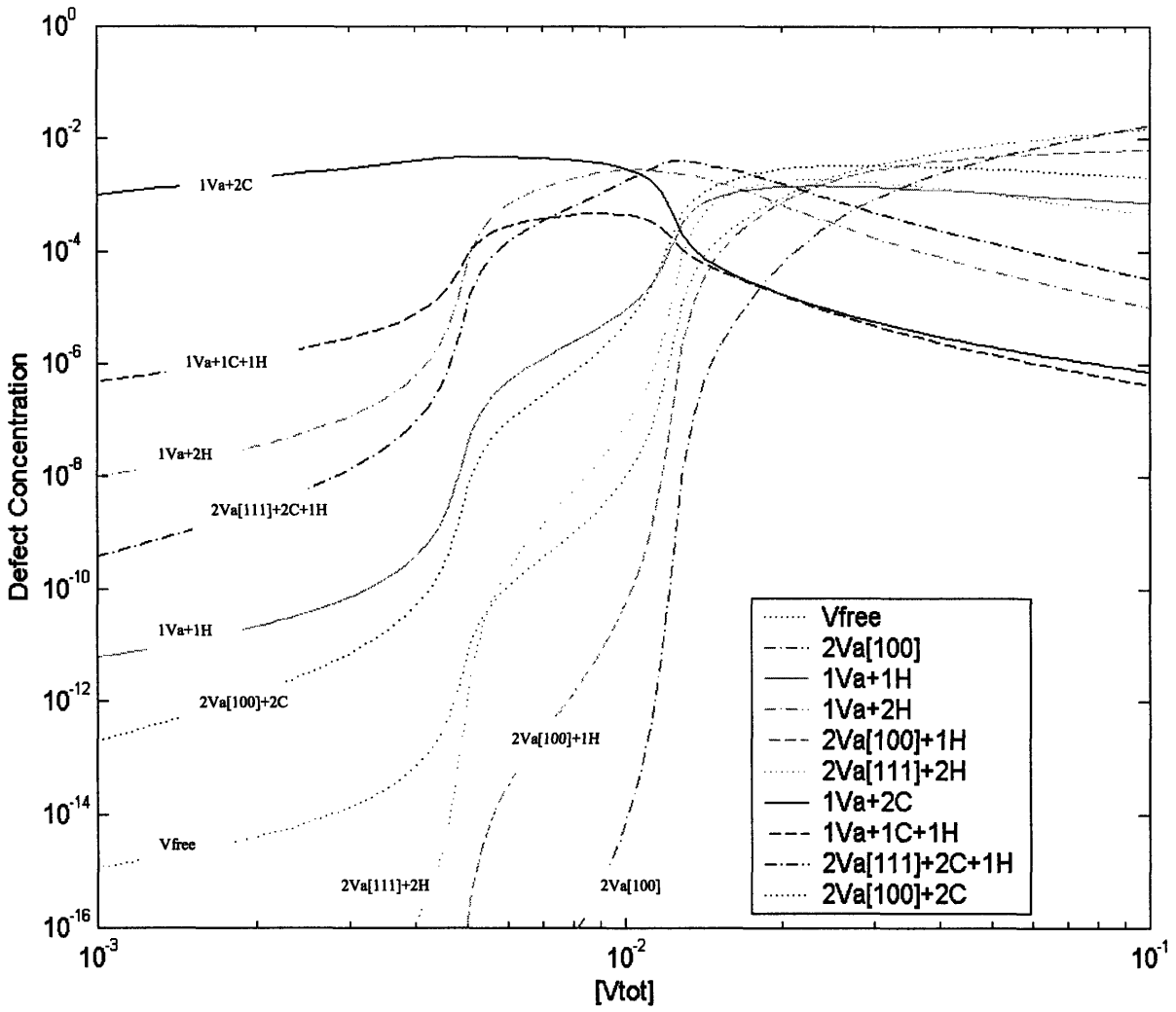

Figure 3.6b. Partial point-defect cluster spectrum in Fe-C-H alloys as a function of total vacancy concentration for $[C_{tot}]=0.01$ and $[H_{tot}]=0.01$. For defects with identical composition only the most statistically significant one is shown. (Magnified version of 3.6.a with C_{oct} and H_{tet} defects not shown for clarity)

The main difference between the high hydrogen content alloy shown in figures 3.6a and 3.6b and the low hydrogen one in figures 3.5.a and 3.5b is the replacement of the 1Va-1C-1H cluster by 2Va-2C-1H and 1Va-2H clusters as the most prevalent hydrogen-containing cluster throughout the entire vacancy concentration range. In fact, in this case the main defect complexes for vacancy concentrations of approximately 0.01 are 2Va-2C-1H and 1V-2H rather than 1Va-2C or 2Va-2C. For $V_{tot} \approx 0.017$, five different types of defect clusters dominate the

spectrum (2Va-2C-1H, 2Va-2C, 1Va-2H, 2Va-2H, and 1Va-1H) corresponding to 4 different stoichiometries. Hence, we expect that in the neighborhood of this composition (1 at. % C, 1 at. % H, and ~1.7 a. % Va) the diffusive behavior will be dominated by multiple migration barriers in a complex fashion.

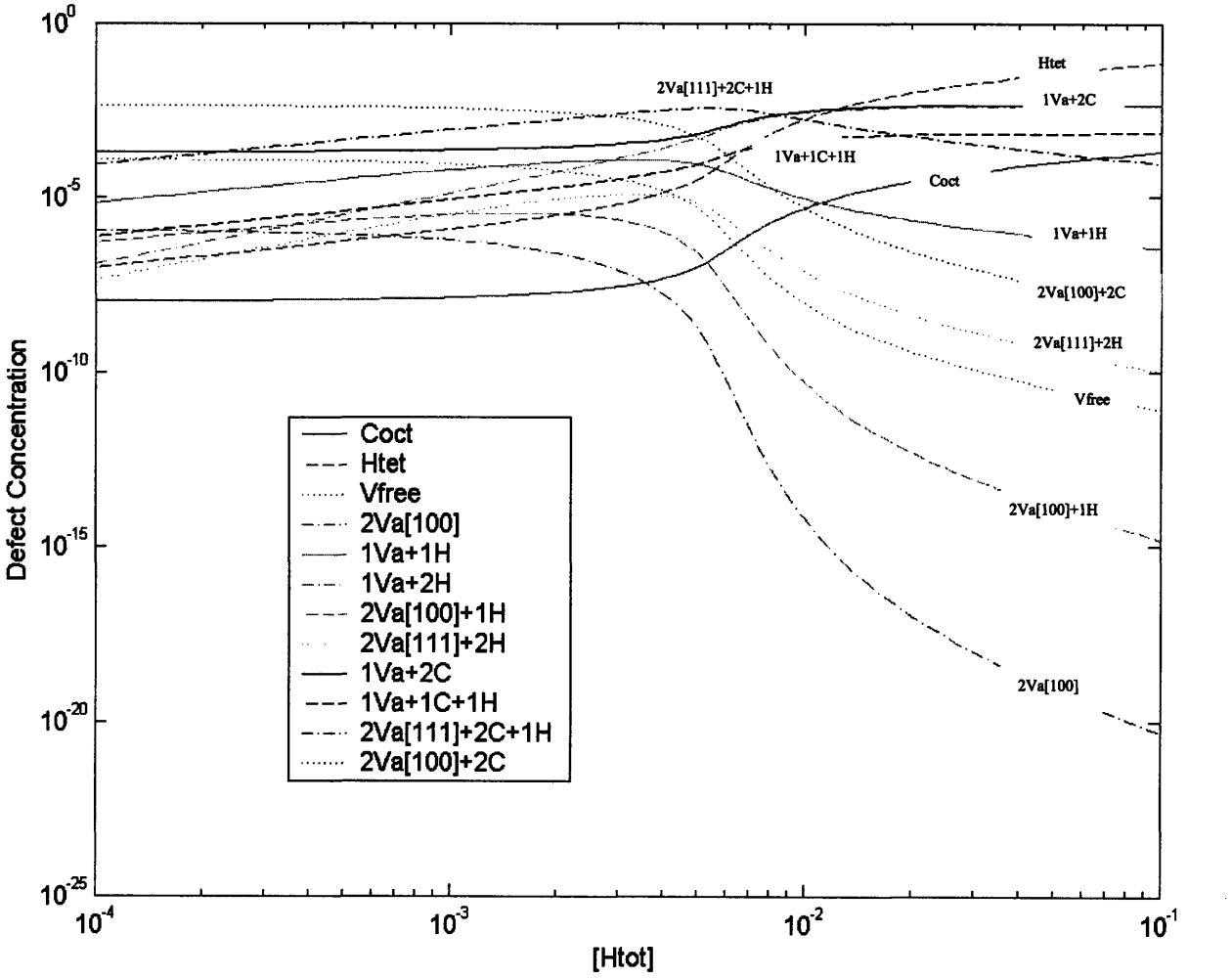

Figure 3.7. Partial point-defect cluster spectrum in Fe-C-H alloys as a function of total hydrogen concentration for $[C_{tot}]=0.01$ and $[V_{tot}]=0.01$. For defects with identical composition only the most statistically significant one is shown.

Figure 3.7 shows the defect concentrations for the complexes from figure 3.6.a as a function of hydrogen concentration with $C_{tot}=V_{tot}=0.01$. We notice that with these values the hydrogen-containing defects dominate the spectrum only when $[H_{tot}] > 0.03$, but even at lower

concentrations, and consistent with previous observations, they remain significant.

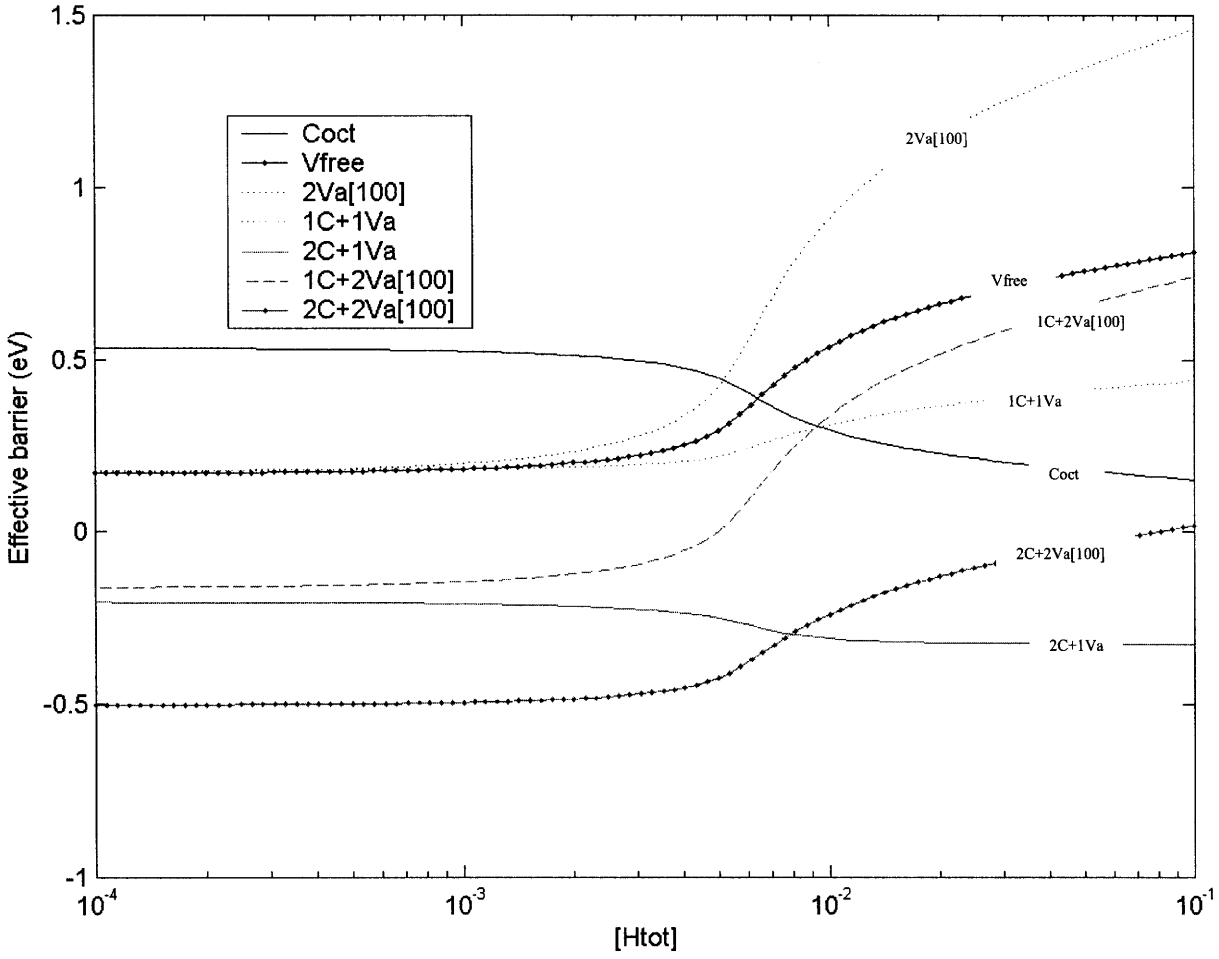

Figure 3.8. Effective activation barriers for key point-defect clusters in Fe-C-H as a function of total hydrogen concentration for $[C_{tot}]=0.01$ and $[V_{tot}]=0.01$.

Also, and in contrast with the previous figures, the critical behavior reflective of the rough energy landscape in figures 3.4-3.6 is essentially absent when the total hydrogen concentration becomes a variable rather than a constraint. This can again be associated with the fact that H-Va, and H-C interactions are weaker than C-Va ones and therefore altering the hydrogen composition does not change the position of the system in energy space as drastically as modifying the vacancy concentration does. In addition, in the plots given in figures 3.5-3.6 we still observe the critical/threshold behavior which characterizes the Fe-C and Fe-H point-defect spectra. However,

the transitions in the ternary system are less sharp in comparison to the Fe-C system only (figure 3.2.). This can be associated with a smoother trajectory in the energy landscape (i.e. with less drastic changes in the effective activation barriers or equivalently less drastic changes of the coordinate in energy space.) which is confirmed by comparing figure 3.8 above with figure 3.3.

3.6. Bulk vs. Local Effects

In section 3.5, the effects of hydrogen on the point-defect spectrum of Fe-C alloys were discussed under the assumption of a homogeneous bulk in which the concentrations of the component species (free vacancies, octahedral carbon interstitials, and tetrahedral hydrogen interstitials) were identical throughout the sample. Under those assumptions we concluded that the point-defect microstructure could undergo drastic changes, if the concentration of hydrogen or of vacancies was increased beyond certain thresholds. However, some of the required concentrations were unfeasibly large for the bulk to attain, e.g. at 160 °C, hydrogen pressures of 23.2 atm and 232 atm were necessary to achieve bulk hydrogen concentrations of 1000 and 10^4 ppm, respectively.

However, realistic materials are not infinitely large and homogeneous. The presence of surfaces as well as localized extended defects such as dislocations, grain boundaries, and cracks can dramatically modify the local properties of the material and the local concentrations of free vacancies and impurity atoms can be orders of magnitude higher in the neighborhood of any extended imperfection than in the bulk. For instance, as highlighted in section 2.4, the binding energy of hydrogen to surfaces, dislocations, and grain boundaries is much higher than that at the point-defect clusters with which we are concerned in this thesis. Hirth [10] indicates that at hydrogen pressures as low as 0.05 Pa and at approximately room temperature, the H concentration at free surfaces and Fe_3C interfaces essentially saturates over 0.966. With an

atmosphere of hydrogen pressure and also at room temperature, grain boundaries and dislocation cores, in addition to free surfaces, saturate in hydrogen. In addition, the concentration of vacancies in the neighborhood of an extended defect is known to be substantially higher than the equilibrium vacancy concentration in the bulk, and a variety of alloying elements are known to diffuse to grain boundaries and interfaces.

In conclusion, even though the results obtained in sections 3.2 to 3.5 may not necessarily be applicable to the homogeneous bulk of the material (though additional sources of vacancies and hydrogen such as cold-working and welding may allow for the concentrations discussed), the results are representative of the point-defect spectrum in the neighborhood of extended defects. Hence, since the mechanical behavior of the material is governed by the interactions of the point-defect complexes with those extended defects, our results continue to have a direct impact in understanding hydrogen induced degradation and can thus be used as the foundation for multi-scale computational approaches.

Chapter 4

4. Multi-scale Approach to Embrittlement and Future Work

The results exposed in chapter 3 represent only the foundation for building a comprehensive multi-scale computational model able to characterize hydrogen embrittlement in steels. A profound understanding of the physical mechanisms which govern the stability, structure, and distribution of point-defect clusters in the presence of hydrogen has been emphasized throughout this work as a key building block in understanding the interactions of hydrogen with extended defects as well as the migration properties of the material which control time-dependent processes such as creep.

Nonetheless, in order to correlate our atomistic results to macroscopic properties it is necessary to develop a methodology that allows us to bridge the numerous length and time scales involved in the problem. With this objective in mind we propose a comprehensive computational approach designed to tackle some of the open questions in hydrogen embrittlement by building upon the work summarized in this thesis.

4.1. Hydrogen Empirical Potentials

The first step towards extending our atomistic approach to larger systems such as dislocations, grain boundaries, and surfaces is to develop an empirical potential for the Fe-H, C-H, and H-H interactions which properly account for the *ab initio* binding and stability results from section 3.2.

Empirical potentials for the Fe-Fe [103] and Fe-C [104] interactions are already available in the literature and produce accurate results when compared to *ab initio* formation energies of the

point-defect clusters of interest. In addition, an embedded atom method (EAM) potential for the Fe-H system has also been fitted by Wen and co-workers [105] to experimental measurements of the binding energies of some Fe-V complexes. However, it is unlikely that Wen's potential would be able to duplicate the defect-stability order predicted by the DFT results since the empirical binding energies represent a coarse-grained average due to the difficulties in the experimental measures.

Furthermore, even if the Fe-H and H-H interactions are accounted for properly by already existing potentials, available H-C potentials are not well suited for the description of our defect microstructure. As such, an important part in extending our results to larger length scales is the development and fitting of new inter-atomic many-body potentials that describe the Fe-C-H system while ranking the different energy minima consistently with our DFT calculations. To this end, we propose the use of the Modified Embedded Atom Method (MEAM) formalism [106] for the potential given its previous success with Fe-C, Fe-Cu, as well as its ability to capture the fundamental quantum mechanical nature of hydrogen binding and diffusion.

4.2. Cluster Migration and KMC Modeling of Dislocation Climb

The next step in the multi-scale methodology involves the study of the diffusive behavior of the system to gain insight into time-dependent phenomena such as creep and other forms of structural relaxation. Thus, we must determine the migration barriers for the most statistically significant clusters found in chapter 3 and then correlate them with analytic models of diffusion and creep.

Using the nudged-elastic band method [107] in conjunction with an appropriate empirical potential (or with DFT calculations and large computational resources) we can then determine the forward and backward barriers for the migration of the prevalent defect complexes. Since the

tunneling transition probability for H migration in Fe is expected to be large, the jumps between neighboring tetrahedral sites should be caused by adiabatic transitions between the ground states [91], and therefore a semi-classical approach using the DFT informed potential should be able to capture the correct diffusion mechanics.

The jump frequencies and diffusivities can then be derived from the barriers by using the Harmonic Transition State Theory derived by Vineyard [108]. The self-diffusivity can then be calculated as:

$$D_{Fe} = \sum_{i \in \{defects\}} a_i^2 [i] v_i^o \exp\left(-\frac{\Delta U_m^i}{kT}\right) f_i \qquad (4.2.1)$$

where a_i is the jump distance, [i] is the concentration of defect i, v_i^o is the jump frequency, ΔU_m^i is the migration activation energy, and f_i is the correlation factor. The sum is, in principle, over all defect clusters. However, since each term is multiplied by the defect concentration, non-statistically significant defect complexes can be ignored. From our results in chapter 3 we can find the concentrations and using the methodology described in this section we can obtain the remaining terms in the equation. Using this approach we can then quantify the effects of various hydrogen concentrations on the material's diffusive behavior. In addition, this approach can be extended to explore the effects of dislocation and crack interactions on the activation barriers as hence on the full diffusivity coefficient.

Finally the migration rates obtained using the NEB approach can be incorporated into kinetic Monte Carlo models of heterogeneous diffusion. The KMC model would then combine traditional approaches to defect diffusion with spatially dependent and *ab initio* informed jump rates obtained from previous stages of the methodology. In addition, by using spatially dependent barriers the model can then explicitly include atomistic resolution onto dislocation cores and could then, in principle, be used to model dislocation climb, glide, and hence creep.

Chapter 5

5. Conclusions

In this thesis we addressed a variety of fundamental questions related to the stability, structure, and concentrations of point defect clusters in Fe-C-H by using atomistic modeling and simulation. We found that both carbon and hydrogen bind strongly to free vacancies, stabilizing them in the form of larger defect clusters. Both hydrogen and carbon sit on interstitial sites of the BCC structure, with carbon preferring octahedral sites while hydrogen sits on the tetrahedral ones.

In addition, in the absence of hydrogen, the spectrum is dominated by 1Va-2C and 2Va-2C defects, while the addition of small concentrations of hydrogen increases the number of statistically significant defects with the 1Va-1C-1H defects becoming one of the dominant defects within a small vacancy range. Higher hydrogen concentrations have a more pronounced effect on the defect cluster population with complexes such 2Va-2C-1H and 1V-2H taking over as the most statistically significant ones once the total hydrogen content is comparable to that of carbon.

Also we find that the various defect spectra are characterized by the presence of sharp critical or threshold transitions when the vacancy concentration is weakly changed and, through the use of an effective activation energy barrier, this behavior can be traced to the presence of deep wells in the free energy landscape as a function of chemical composition. Changes in the vacancy concentration have a much more pronounced effect on the concentration than changes in the hydrogen content because H-Va and C-Va bonds are much stronger than C-H bonds. Thus altering the vacancy concentration represents a more drastic change in the reaction coordinate in energy space and hence in the effective activation barrier.

Furthermore, we concluded that the drastic changes in the defect concentrations would not take place in the bulk under normal hydrogen pressures. However, they can easily occur in the neighborhood of extended defects such as dislocations and surfaces in which the local hydrogen and vacancy concentrations are orders of magnitude higher and can thus have a pronounced effect on the interactions with those extended defects, which in turn dominate the mechanical response of the material.

Finally, we proposed a multi-scale modeling framework coupling Nudged Elastic Band and Kinetic Monte Carlo techniques to our results. Through this methodology we can expand the scope of our calculations to the study the greater problem of hydrogen embrittlement and other hydrogen-induced phenomena in steels and other Fe-based alloys, which is of great technological and scientific relevance.

References

[1] M. Paesler, S. C. Agarwal, and R. Zallen, Eds., *Proceedings of the 13th International Conference on Amorphous and Liquid Semiconductors*, J. Non-Cryst. Solids **114** (1989).

[2] E. H. Poindexter, Ed., *Metal-Oxide-Semiconductor Structures,* Semicond. Sci. Technol. **4**, 970 (1989).

[3] K. K. Schuegraf, 1988, Ed., *Handbook of Thin-Film Deposition Processes and Techniques* (Noyes, Park Ridge, NJ).

[4] J. C. Angus and C. C. Hayman, Science **241**, 913 (1988)

[5] P. K. Bachmann and R. Messier, 1989, Chem. Eng. News, May 15, p. 24 (special report)

[6] Y. Fukai and N. Okuna, Jpn. J. Appl. Phys., Part 2 **32**, L1256 (1993)

[7] M. Iwamoto and Y. Fukai, Mater. Trans., JIM **40**, 6060 (1999)

[8] E. Hayashi, Y. Kurokawa, and Y. Fukai, Phys. Rev. Lett. **80**, 5588 (1998).

[9] Y. Fukai and N. Okuma, Phys. Rev. Lett. **73**, 1640 (1994).

[10] J. P. Hirth. Metall. Trans. A. 11A (1980).

[11] M. Nagumo, M. Nakamura, and K. Takai. Metall. Mater. Trans. A, 32A, pp. 339-347 (2001).

[12] T. N. Veziroglu: *Proceedings of the Hydrogen Economy Energy Conference*, University of Miami, Coral Gables, FL, 1974.

[13] R. A. Oriani. Ann. Rev. Mater. Sci., 1978, vol 8, pp. 327-357.

[14] I. M. Bernstein and A. W. Thompson, eds., *Hydrogen in Metals*, ASM, Metals Park, OH, 1974.

[15] A. W. Thompson and I. M. Bernstein, eds., *Effect of Hydrogen on Behavior of Materials,* TMS-AIME, New York, 1976.

[16] R. W. Staehle, J. Hochmann, R. D. McCright, and J. E. Slater, eds., *Stress Corrosion Cracking and Hydrogen Embrittlement of Iron Base Alloys*, NACE-5, NACE, Houston, TX, 1977.

[17] P. Bastien, ed., *L'Hydrogene dans Les Metaux.* Vols. 1 and 2, Editions Sci. Et Ind., Paris, 1972.

[18] *Proceedings of the 2nd International Conference on Hydrogen in Metals, Paris, 1977*, vols. 1-10, Pergamon, Oxford, 1978.

[19] I.M. Robertson, Engineering Fracture Mechanics, 64, 1999, pp. 649-673.

[20] P. Sofronis, Y. Liang, N. Aravas, Eur. J. Mech. A/Solids, 20, 2001, pp.857-872.

[21] Y. Liang, P. Sofronis, N. Aravas, Acta Materialia, 51, 2003, pp.2717-2730.

[22] M. Nagumo, K. Takai, N. Okuda, J. Alloys and Compounds, 293-295, 1999, pp.310-316.

[23] M. Nagumo, K. Ohta, H. Saitoh, Scripta Materialia, Vol. 40, No. 3, 1999, pp. 313-319.

[24] M. Nagumo, ISIJ International, Vol. 41, 2001, No. 6, pp. 590-598.

[25] M. Nagumo, T. Ishikawa, T. Endoh, Y. Inoue, Scripta Materialia, 49, 2003, pp. 837-842.

[26] Y. Fukai, J. Alloys and Compounds, 356-357, 2003, pp. 263-269.

[27] C. Först, J. Slycke, K. Van Vliet, and S. Yip. Phys. Rev. Lett. 96, 175501 (2006).

[28] A. Vehanen, P. Hautojarvi, J. Hohannson, J. Yli-Kauppila, and P. Moser. Phys. Rev. B 26, 762 (1982).

[29] J. Wilde, A. Cerezo, and G. D. Smith, Scripta Materialia. 43, 39 (2000).

[30] B. T. A. McKee, W. Triftshuser, and A. T. Stewart, Phys. Rev. Lett. 28, 358 (1972).

[31] T. T. Lau, X. Lin, K. Van Vliet, and S. Yip, Unpublished results.

[32] D. E. Jiang and E. A. Carter, Phys. Rev. B 67, 213103 (2003).

[33] D. A. Jones, 1996, *Principles and Prevention of Corrosion*. (Upper Saddle River, NJ).
[34] W. H. Johnson. Proc. Roy. Soc. London 23 (1875), (reproduced in "Hydrogen damage"). American Society for Metals, Ohio, 1977.
[35] I. M. Robertson. Engineering Fracture Mechanics, 68, 2001, pp. 671-692.
[36] C. Zapffe. Trans. American Society for Metals 1947; 39; 191-192.
[37] F. Kazinczy. Journal of the Iron and Steel Institute, 177, 1954, pp. 85-92.
[38] N. J. Petch. Nature, 169 (1952), pp. 842-843.
[39] N. J. Petch. Phil. Mag. 1 (1956), pp. 331-335.
[40] J. G. Morlet, H. H. Johnson, A. R. Troaiano. Jounral of the Iron and Steel Institute, 189, 1958, pp. 37-41.
[41] A. R. Troiano. Trans. ASM 1960; 52; 54-80.
[42] G. M. Pressouyre, I. M. Bernstein. Metall. Trans. A, 9A, 1571 (1978).
[43] G. M. Pressouyre, I. M. Bernstein. Acta Metall, 27 (1979) pp. 89-100.
[44] G. M. Pressouyre. Acta. Metall, 28 (1980) pp. 895-911.
[45] D. N. Williams. J. Inst. Metals, 91, 147 (1963).
[46] R. H. Windle, G. C. Smith. Mater. Sci. J., 2, pp. 187-191 (1968).
[47] M. Cornet, M. F. Trichet, S. Talbot-Bernard, Memoires Scientifiques de la Revue de Metallurgie 1977; 74, pp. 307-316.
[48] C. D. Beachem. Metall. Trans. A, 3, 437 (1972).
[49] S. P. Lynch. Met. Forum, 2, pp. 189-200 (1979).
[50] J. Eastman, F. Heubaum, T. Matsumoto, H. K. Birnbaum. Acta Metall., 30, pp. 1579-1586 (1982).
[51] T. H. Maugh, Science, 178 (1972) 849.
[52] T. Kawai, and T. Sakata, Nature, 286, 474-476 (1980).
[53] J. Norbeck, et al. *Hydrogen Fuel for Surface Transportation*. Warrendale, PA: Society of Automotive Engineers, 1996.
[54] J. M. Ogden, Physics Today, 55, pp. 69-75 (2002).
[55] R. B. McLellan, and C. G. Harkins. Mat. Sci. and Eng 18 (1975) 5-35.
[56] R. B. McLellan and W. A. Oates, Acta Met., 21 (1973) 181.
[57] R. B. McLellan, in P.S. Rudman, J. Stringer and R. I. Jaffee (Eds.), Phase Stability in Metals and Alloys, McGraw-Hill, New York, 1967.
[58] N. R. Quick and H. H. Johnson, Acta Met., vol. 26, pp. 903-907 (1976).
[59] R. A. Oriani: *Fundamental Aspects of Stress-Corrosion Cracking,* NACE-1, pp. 32-49, NACE, Houston, TX, 1969.
[60] M. R. Louthan, Jr., et al: Ref 15, pp. 337-447.
[61] R. A. Oriani, Ann. Rev. Mater. Sci., vol. 8, pp. 327-257 (1978).
[62] C. D. Beachem, Metall. Trans., Vol. 3 (1972) pp. 437-451.
[63] J. P. Hirth. *Environment Sensitive Fracture of Metals and Alloys,* Proc. Office of Naval Research Workshop, Washington D.C. , June 3-4, 1985, Office of Naval Research, Arlington, VA, p. 79, 1987.
[64] H. K. Birnbaum. *Environment Sensitive Fracture of Metals and Alloys,* Proc. Office of Naval Research Workshop, Washington D.C. , June 3-4, 1985, Office of Naval Research, Arlington, VA, p. 105, 1987.
[65] G. Lu, et al. Phys. Rev. Lett., 87, 095501 (2001).
[66] G. Lu, et al. Phys. Rev. B, 65, 064102 (2002).
[67] V. G. Gavriljuk, et al., Scripta Materialia, 34, No. 6, pp. 903-907 (1996).

[68] R. B. McLellan, Z. R. Xu. Scripta Materialia, 36, No. 10, pp. 1201-1205 (1997).
[69] Yu. Jagodzsinski, et al, Scripta Materialia, Vol. 43, 2000, pp. 245-251
[70] T. Matsumoto, J. Eastman, and H. K. Birnbaum, Scripta Metall., 15 (1981) 1033.
[71] H. K. Birnbaum and P. Sofronis, Mat. Sci. and Eng. A176 (1994) 191-202.
[72] R. B. McLellan, Acta Met., 1979, vol. 27, pp. 1655-64.
[73] S. M. Myers, et al. Rev. Mod. Phys., Vol. 64, No. 2 (1992).
[74] Y. Tateyama, and T. Ohno. ISIJ International, Vol. 43 (2003), No. 4, pp. 573-578.
[75] Y. Tateyama, and T. Ohno. Phys. Rev. B 67, 174105 (2003).
[76] J. K. Nørskov, and F. Besenbacher, J. Less-Common Met. 130, 475 (1987).
[77] J. A. Brown, R. H. Heffner, M. Leon, and M. E. Schillaci, Phys. Rev. Lett. 43, 1513 (1979).
[78] M. E. Pronsato, C. Pistonesi, and A. Juan, J. Phys. Condens. Matter 16 (2004) 6907-6916.
[79] S. M. Myers, S. T. Picraux, and R. E. Stoltz, J. Appl. Phys. 50, 5710 (1979).
[80] S. T. Picraux, Nucl. Instrum. Methods 182-183, 413 (1981).
[81] J. K. Nørskov, et al. Phys. Rev. Lett. 49, 1420 (1982).
[82] A. I. Shirley, and C. K. Hall, Scr. Metall. 17, 1003 (1983).
[83] A. I. Shirley, and C. K. Hall, Acta Metall. 32, 49 (1984).
[84] A. I. Shirley, C. K. Hall, and N. J. Prince, Acta Metall. 31, 985 (1983).
[85] P. Hohenberg, and W. Kohn, Phys. Rev. 136, B864 (1964).
[86] W. Kohn and L. J. Sham, Phys. Rev. 140, A1133 (1965).
[87] J. P. Perdew, K. Burke, and M. Ernzerhof, Phys. Rev. Lett. 77, 3865 (1996).
[88] D. E. Jiang, and E. A. Carter, Phys. Rev. B 67, 214103 (2003).
[89] C. Domain, and C. S. Becquart, Phys. Rev. B 65, 024103 (2002).
[90] C. Domain, C. S. Becquart, and J. Foct, Phys. Rev. B 69, 144112 (2004).
[91] Y. Fukai and H. Sugimoto. Advances in Physics, 34:2, 263-326 (1985).
[92] Y. Fukai, and H. Sugimoto. Hydrogen in Metals. Sendai: Japan Institute of Metals. p. 41 (1980).
[93] H. Sugimoto, and Y. Fukai. Phys. Rev. B, 22, 670 (1980).
[94] Y. Fukai. Jap. J. Appl. Phys., 22, 207 (1983), Jap. J. Appl. Phys., 23, L596 (1984).
[95] H. Sugimoto, J. Phys. Soc. Jpn., 53, 2592 (1985).
[96] G. Kresse and J. Furthmuller, Phys. Rev. B 54, 11 169 (1996).
[97] G. Kresse and D. Joubert, Phys. Rev. B 59, 1758 (1999).
[98] P. E. Blöchl. Phys. Rev. B 50, 17953 (1994).
[99] P. E. Blöchl, C. J. Först, and J. Schimpl, Bull. Mater. Sci. 26, 33 (2003).
[100] M. Methfessel, and A. T. Paxton, Phys. Rev. B 40, 3616 (1989).
[101] H. D. Carstanjen, Phys. Status Solidi A, 59, 11 (1980).
[102] C. G. Chen and H. K. Birnbaum, Phys. Status Solidi, 36a, 687 (1976); J. J. Au and H. K. Birnbaum, Acta Met., 26, 1105 (1978).
[103] M. W. Finnis, and J. E. Sinclair, Phil. Mag. A 50, 45 (1984).
[104] T. T. Lau, et al., Phys. Rev. Lett. 98, 215501 (2007).
[105] M. Wen, X.-J. Xu, S. Fukuyama, and K. Yokogawa. J. Mater. Res., Vol. 16, No. 12 (2001).
[106] M. I. Baskes, Phys. Rev. B, 46, 5 (1992).
[107] H. Jónsson, G. Mills, and K. W. Jacobsen, in *Classical and Quantum Dynamics in Condensed Phase Simulations*, B. J. Berne, G. Ciccotti, and D. F. Coker (eds.), World Scientific Publishing Company, 1998, p. 385.
[108] G. H. Vineyard, J. Phys. Chem. Solids, 3, 121 (1957).